J. Fluid Mech. (2005), *vol.* 530, *pp.* 145–176. © 2005 Cambridge University Press
doi:10.1017/S002211200500368X Printed in the United Kingdom

A model for the nonlinear dynamics of turbulent shear flows

By PASCALE GARAUD[1,2] AND GORDON I. OGILVIE[1,2]

[1]Institute of Astronomy, University of Cambridge, Madingley Road, Cambridge CB3 0HA, UK

[2]Department of Applied Mathematics and Theoretical Physics, Centre for Mathematical Sciences, University of Cambridge, Wilberforce Road, Cambridge CB3 0WA, UK

(Received 21 April 2004 and in revised form 2 November 2004)

We investigate the nonlinear dynamics of turbulent shear flows, with and without rotation, in the context of a simple but physically motivated closure of the equation governing the evolution of the Reynolds stress tensor. We show that the model naturally accounts for some familiar phenomena in parallel shear flows, such as the subcritical transition to turbulence at a finite Reynolds number and the occurrence of a universal velocity profile close to a wall at large Reynolds number. For rotating shear flows we find that, depending on the Rayleigh discriminant of the system, the model predicts either linear instability or nonlinear instability or complete stability as the Reynolds number is increased to large values. We investigate the properties of Couette–Taylor flows for varying inner and outer cylinder rotation rates and identify the region of linear instability (similar to Taylor's), as well as regions of finite-amplitude instability qualitatively compatible with recent experiments. We also discuss quantitative predictions of the model in comparison with a range of experimental torque measurements. Finally, we consider the relevance of this work to the question of the hydrodynamic stability of astrophysical accretion disks.

1. Introduction

Turbulent motion in the flow of an incompressible fluid has consistently eluded a satisfying mathematical description in over a century of investigation. The governing Navier–Stokes equations, although involving only a relatively simple nonlinearity, conceal a remarkable wealth of complex behaviour. Even in the simplest problem of the onset of turbulent motion in a parallel shear flow, the classical approach based on a linear analysis of normal modes fails spectacularly to account for the basic experimental results (e.g. Drazin & Reid 1981). A better insight into the transition to turbulence has been gained more recently through studies of the transient amplification of disturbances in linear theory (Butler & Farrell 1992), which, when coupled with an appropriate nonlinear feedback, allows perturbations to be sustained (e.g. Baggett & Trefethen 1997). The direct computation of nonlinear disturbances in the form of (possibly unstable) steady solutions or travelling waves that act as precursors of the turbulent dynamics (Nagata 1990; Waleffe 1997) has also shed light on the process of transition.

By its nature, fully developed turbulence demands a statistical description. Reynolds (1895) established the principles of a statistical theory, showing that correlations between components of the fluctuating velocity field provide a stress that influences the bulk motion. The analogy between this turbulent transport of momentum and the viscous transport associated with thermal molecular motion in kinetic theory

https://doi.org/10.1017/S002211200500368X Published online by Cambridge University Press

suggested the concept of eddy viscosity, introduced by Boussinesq (1877). Later, Prandtl's (1925) theory of the mixing length gave a predictive expression for the eddy viscosity that provided a remarkable quantitative agreement with experimental data such as the mean flow rate in turbulent pipe flow (Schlichting 1979).

Despite the success of mixing-length theory, much effort has been expended in a search for more accurate representations of the Reynolds stress in turbulent flows, especially in engineering applications. As reviewed by Speziale (1991), the more successful approaches start from the exact equation governing the evolution of the Reynolds stress and apply a procedure of closure modelling to deal with the numerous intractable terms that arise. Through successive algebraic development accompanied by a large number of parameters, such models are able to fit an increasing range of experimental or numerical results. However, in our view, one disadvantage of this approach in its current state is a loss of physical interpretation of those terms derived from complicated algebraic constructions. Moreover, as noted by Speziale (1991), some of these models tend to perform poorly in situations for which they were not calibrated, such as rotating shear flows.

Astrophysics provides examples of naturally occurring shear flows in which rotation is an essential feature. Accretion disks (e.g. Pringle 1981) are usually thin disks of gas in circular orbital motion around a central star or black hole, and are involved in the processes of star and planet formation as well as being responsible for some of the most luminous sources in the Universe. According to Kepler's third law, the angular velocity of the gas depends on the distance from the centre as $\Omega \propto r^{-3/2}$, and an outstanding question of potentially profound significance is whether hydrodynamic turbulence occurs in these situations (e.g. Balbus & Hawley 1998). While it is true that the Reynolds number is exceedingly large ($Re > 10^{14}$; Frank, King & Raine 2002), nevertheless the centrifugal instability of Rayleigh (1917) does not occur because the specific angular momentum $r^2\Omega$ increases outwards (the same criterion was derived by Solberg for homentropic compressible fluids; see Tassoul 1978), and no other suitable hydrodynamic instability has been identified.

Historical experiments by Taylor (1923, 1936*a*, *b*) and Wendt (1933) on Couette–Taylor flow between differentially rotating cylinders have been adduced in the hope of a resolution of this issue (Richard & Zahn 1999). The experiments suggest that turbulence can be sustained even in certain apparently Rayleigh-stable situations such as a Couette–Taylor flow in which only the outer cylinder rotates. In this case the turbulent state is presumably accessed through a nonlinear shear instability of the laminar state associated with a subcritical bifurcation, but the wider applicability of this finding is not well understood. The situation is not helped by the dearth of modern experiments and the fact that Taylor's findings have been challenged by Schultz-Grunow (1959).

In this paper we investigate the nonlinear dynamics of turbulent shear flows, with and without rotation, in the context of a simple but physically motivated closure of the Reynolds-stress equation. Our approach differs from that of the conventional closure models used in engineering applications. We aim to study a minimal system in which the modelled nonlinear terms have a clear interpretation and are as few in number as is compatible with the physical requirements. Indeed, in astrophysical applications the added complexity of other physical processes (convection, magnetic fields, radiative transfer, etc.) forbids anything but a minimal approach in turbulence modelling. In the present context of purely hydrodynamic turbulence this approach allows us to explore the dynamical and nonlinear behaviour in some detail without losing sight of the physical problem.

https://doi.org/10.1017/S002211200500368X Published online by Cambridge University Press

The remainder of this paper is organized as follows. We formulate the model in § 2. Next, in § 3, we examine the local properties of the model in the contexts of homogeneous shear turbulence, with and without rotation, and turbulent shear flow past a wall. We also compare the model with others available in the literature. Section 4 concerns the problem of Couette–Taylor flow. The results are summarized and discussed in § 5.

2. A simple Reynolds-stress model for turbulent shear flows

The flow of an incompressible fluid is governed by the Navier–Stokes equations

$$(\partial_t + u_j \partial_j) u_i = -\partial_i p + \nu \partial_{jj} u_i, \tag{2.1}$$

$$\partial_i u_i = 0, \tag{2.2}$$

where u_i is the velocity, p is the modified pressure (being the pressure divided by the uniform density ρ, plus the gravitational potential), ν is the uniform kinematic viscosity, and we make use of the Cartesian tensor notation. Following a standard technique, the velocity and pressure may be separated into mean and fluctuating parts, e.g.

$$u_i = \bar{u}_i + u_i', \qquad \langle u_i' \rangle = 0, \tag{2.3}$$

where the angle brackets denote a suitable averaging procedure. We readily obtain the averaged Navier–Stokes equations,

$$(\partial_t + \bar{u}_j \partial_j) \bar{u}_i = -\partial_i \bar{p} + \nu \partial_{jj} \bar{u}_i - \partial_j R_{ij}, \tag{2.4}$$

$$\partial_i \bar{u}_i = 0, \tag{2.5}$$

where

$$R_{ij} = \langle u_i' u_j' \rangle \tag{2.6}$$

is the Reynolds-stress tensor divided by the density.

From the fluctuating parts of the Navier–Stokes equations it is possible to obtain an exact equation for R_{ij} in the form

$$\begin{aligned}(\partial_t + \bar{u}_k \partial_k) R_{ij} + R_{ik} \partial_k \bar{u}_j + R_{jk} \partial_k \bar{u}_i - \nu \partial_{kk} R_{ij} \\ = -2\nu \langle (\partial_k u_i')(\partial_k u_j') \rangle - \langle u_i' u_k' \partial_k u_j' + u_j' u_k' \partial_k u_i' \rangle - \langle u_i' \partial_j p' + u_j' \partial_i p' \rangle.\end{aligned} \tag{2.7}$$

There is no difficulty in retaining the exact form of the linear terms on the left-hand side of this equation, which represent the advection of the turbulent fluctuations by the mean flow, their interaction with the mean velocity gradient and the viscous diffusion of the Reynolds stress. The difficult terms on the right-hand side cannot be written exactly in terms of R_{ij}, unless further information is known about the turbulence, and therefore require a closure model. However, the physical effects of these terms are quite well understood and this insight can be used as a guide in constructing the model. In particular, the viscous term on the right-hand side is negative definite and causes a dissipation of the turbulent kinetic energy at a rate that is usually considered to be independent of ν in the limit of large Reynolds number. The other terms are conservative but allow for a redistribution of energy among the components of R_{ij}, and it is well established that anisotropic turbulence has a tendency to return to isotropy (e.g. Rotta 1951).

Recently, one of us proposed a simple model of the stresses in astrophysical magnetohydrodynamic turbulence (Ogilvie 2003). In the special case of hydrodynamic

https://doi.org/10.1017/S002211200500368X Published online by Cambridge University Press

turbulence in an incompressible fluid, the model reduces to the simpler form

$$(\partial_t + \bar{u}_k\partial_k)R_{ij} + R_{ik}\partial_k\bar{u}_j + R_{jk}\partial_k\bar{u}_i = -\frac{C_1}{L}R^{1/2}R_{ij} - \frac{C_2}{L}R^{1/2}\left(R_{ij} - \tfrac{1}{3}R\delta_{ij}\right), \qquad (2.8)$$

where $R = R_{ii}$ is the mean-square turbulent velocity, C_1 and C_2 are positive dimensionless constants of order unity, and L is a characteristic length scale related to the geometrical constraints that limit the size of coherent structures. This model was intended to represent the typical astrophysical situation in which the Reynolds number is exceedingly large and there are no solid surfaces on which boundary layers may form. The modelled nonlinear terms represent two well-known physical processes that are essential in the dynamics of turbulent shear flows. The C_1 term represents the viscous dissipation of turbulent motion, at a rate related to the characteristic time scale $L/R^{1/2}$ of the largest eddies. The C_2 term, which only redistributes energy among the components of R_{ij}, represents the tendency of the turbulence to return to isotropy on a similar time scale. This formulation gives arguably the simplest nonlinear model involving these two essential effects, which also guarantees that the Reynolds tensor remains positive definite and therefore realizable by a genuine velocity field.

In the present paper we are interested in applying the model to laboratory shear flows in which the Reynolds number is not exceedingly large and in which boundary layers are present. We therefore enhance the model by retaining the viscous diffusion of the Reynolds stress and including an additional term to model viscous dissipation on the right-hand side:

$$\begin{aligned}(\partial_t + \bar{u}_k\partial_k)R_{ij} + R_{ik}\partial_k\bar{u}_j + R_{jk}\partial_k\bar{u}_i - \nu\partial_{kk}R_{ij} \\ = -\frac{C_1}{L}R^{1/2}R_{ij} - \frac{C_2}{L}R^{1/2}\left(R_{ij} - \tfrac{1}{3}R\delta_{ij}\right) - \frac{C_\nu\nu}{L^2}R_{ij}. \qquad (2.9)\end{aligned}$$

Here C_ν is a third positive dimensionless constant of order unity, and the C_ν term allows for the fact that, at low or moderate Reynolds numbers, when an efficient turbulent cascade does not form, the viscous dissipation rate is directly proportional to the viscosity. Hence in what follows, although we often denote as 'turbulent' any flow for which $R > 0$, the Reynolds stresses for relatively low Reynolds numbers are more likely to represent the average behaviour of large-scale coherent structures (such as Taylor vortices in the case of the Couette–Taylor system). Wavelike behaviour, on the other hand, cannot be well represented in this formalism owing to the assumed locality of the dissipation.

In the original model L was related to the thickness of an accretion disk; in a stratified atmosphere it might be related to the density scale height. It was not necessary to give a precise definition of L owing to the invariance of the original model under a rescaling

$$L \mapsto \lambda L, \qquad C_1 \mapsto \lambda C_1, \qquad C_2 \mapsto \lambda C_2. \qquad (2.10)$$

In the present paper, however, we will make a definite choice for L appropriate to the geometrical constraints of the problem, and we will attempt to fix the values of the coefficients by comparison with experimental results.

It is straightforward, as in Ogilvie (2003), to allow for a uniform rotation of the frame of reference with angular velocity Ω_i. In this case we obtain additional Coriolis terms of the form

$$(\partial_t + \bar{u}_k\partial_k)R_{ij} + R_{ik}\partial_k\bar{u}_j + R_{jk}\partial_k\bar{u}_i + 2\epsilon_{jkl}\Omega_k R_{il} + 2\epsilon_{ikl}\Omega_k R_{jl} + \cdots. \qquad (2.11)$$

https://doi.org/10.1017/S0022112005003680X Published online by Cambridge University Press

The expression for the Reynolds-stress equation (2.8) in a general orthogonal curvilinear coordinate system is given in Appendix A, together with an explicit expression for $\partial_{kk} R_{ij}$ in cylindrical polar coordinates.

3. Local properties of the model

3.1. *Homogeneous shear turbulence*

We first consider the idealized situation of a uniform shear flow,

$$\bar{\boldsymbol{u}} = Sy\,\boldsymbol{e}_x, \tag{3.1}$$

where (x, y, z) are Cartesian coordinates and the shear rate S is prescribed. We also allow for a uniform rotation of the frame of reference with angular velocity

$$\boldsymbol{\Omega} = \Omega\,\boldsymbol{e}_z. \tag{3.2}$$

We assume that the geometrical constraints are such that L is constant. This can be achieved by performing a numerical simulation in a periodic box with no solid boundaries (Rogallo 1981; Pumir 1996), in which case L is related to the size of the box. This system is the only one in which the size of the coherent structures can be limited without imposing additional boundary conditions that would result in the loss of the large-scale homogeneity of the flow. The turbulence may therefore be assumed to be statistically homogeneous, although it is anisotropic. In this case the Reynolds stress depends only on time and the model reduces to a system of ordinary differential equations constituting an autonomous nonlinear dynamical system. We find, in detail,

$$\left.\begin{aligned}
&\partial_t R_{xx} + 2(S-2\Omega)R_{xy} = -\frac{(C_1+C_2)}{L}R^{1/2}R_{xx} + \frac{C_2}{3L}R^{3/2} - \frac{C_\nu \nu}{L^2}R_{xx},\\
&\partial_t R_{xy} + 2\Omega R_{xx} + (S-2\Omega)R_{yy} = -\frac{(C_1+C_2)}{L}R^{1/2}R_{xy} - \frac{C_\nu \nu}{L^2}R_{xy},\\
&\partial_t R_{xz} + (S-2\Omega)R_{yz} = -\frac{(C_1+C_2)}{L}R^{1/2}R_{xz} - \frac{C_\nu \nu}{L^2}R_{xz},\\
&\partial_t R_{yy} + 4\Omega R_{xy} = -\frac{(C_1+C_2)}{L}R^{1/2}R_{yy} + \frac{C_2}{3L}R^{3/2} - \frac{C_\nu \nu}{L^2}R_{yy},\\
&\partial_t R_{yz} + 2\Omega R_{xz} = -\frac{(C_1+C_2)}{L}R^{1/2}R_{yz} - \frac{C_\nu \nu}{L^2}R_{yz},\\
&\partial_t R_{zz} = -\frac{(C_1+C_2)}{L}R^{1/2}R_{zz} + \frac{C_2}{3L}R^{3/2} - \frac{C_\nu \nu}{L^2}R_{zz}.
\end{aligned}\right\} \tag{3.3}$$

It can easily be seen that the two components R_{xz} and R_{yz} are decoupled from the others; these quantities may be expected to vanish on grounds of symmetry, as is confirmed below.

The system is characterized by a Reynolds number

$$Re = \frac{L^2|S|}{\nu} \tag{3.4}$$

and an inverse Rossby number

$$Ro^{-1} = \frac{2\Omega}{S}. \tag{3.5}$$

The Rayleigh discriminant of the rotating shear flow is

$$\Phi = 2\Omega(2\Omega - S). \tag{3.6}$$

https://doi.org/10.1017/S002211200500368X Published online by Cambridge University Press

We recall that $\Phi < 0$ is a sufficient condition for the instability of a rotating shear flow in the absence of viscosity. We refer informally to the situations $\Phi < 0$, $\Phi = 0$ and $\Phi > 0$ as 'Rayleigh-unstable', 'Rayleigh-neutral' and 'Rayleigh-stable' even though the criterion is limited in its strict applicability. It is convenient to define a dimensionless Rayleigh discriminant

$$\phi = Ro^{-1}(Ro^{-1} - 1) \tag{3.7}$$

and a Taylor number

$$Ta = -Re^2\phi. \tag{3.8}$$

The dynamical system (3.3) possesses a trivial fixed point, $R_{ij} = 0$, which represents the laminar state. Linear analysis indicates that the trivial fixed point is unstable with respect to infinitesimal perturbations when the Taylor number exceeds a positive critical value,

$$Ta > Ta_c = \frac{C_\nu^2}{4}. \tag{3.9}$$

Although a linear instability of this kind is possible only in Rayleigh-unstable situations, we demonstrate below that turbulent states can be accessed through a nonlinear instability of the laminar state under a wider range of conditions.

The dynamical system may also possess non-trivial fixed points, representing states of statistically steady and homogeneous turbulence in which viscous dissipation is compensated by an extraction of energy from the shear flow. Such states may be either stable or unstable; even if it does not represent a statistical endpoint of the dynamics, an unstable solution may play a transient role in the dynamics by providing an organizing structure in the dynamical phase space. Searching for non-trivial fixed points, we obtain the condition

$$\frac{2C_2}{3L}S^2R^{1/2} = \left\{\left[\frac{(C_1+C_2)}{L}R^{1/2} + \frac{C_\nu\nu}{L^2}\right]^2 + 8\Omega(2\Omega - S)\right\}\left[\frac{C_1}{L}R^{1/2} + \frac{C_\nu\nu}{L^2}\right], \tag{3.10}$$

which may be written as a cubic equation for the dimensionless r.m.s. turbulent velocity $u = R^{1/2}/L|S|$,

$$\frac{2C_2}{3}u = \left\{\left[(C_1+C_2)u + \frac{C_\nu}{Re}\right]^2 + 4\phi\right\}\left(C_1u + \frac{C_\nu}{Re}\right). \tag{3.11}$$

The behaviour of u as a function of Re depends on the dimensionless Rayleigh discriminant ϕ of the rotating shear flow. In the present model two values of ϕ with special significance are

$$\phi_- = -\frac{C_2}{12(C_1+C_2)}, \qquad \phi_+ = \frac{C_2}{6C_1}. \tag{3.12}$$

Excluding degenerate intermediate cases, we identify four intervals of interest and illustrate in figure 1 the corresponding bifurcation diagrams in which u is plotted against Re. Although the qualitative features of the set of bifurcation diagrams do not depend on the parameters C_1, C_2 and C_ν, we make a particular selection of 'standard' parameters which is explained in § 3.4 below.

(*a*) $-\frac{1}{4} \leqslant \phi < \phi_-$. As Re is increased, the laminar state loses stability to a branch of turbulent solutions at a supercritical bifurcation.

https://doi.org/10.1017/S002211200500368X Published online by Cambridge University Press

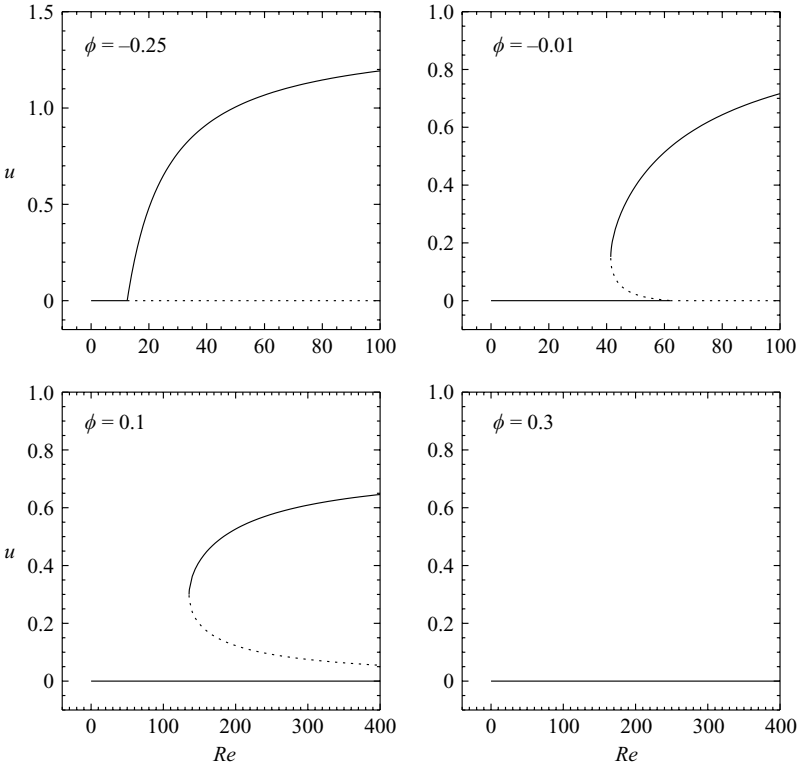


FIGURE 1. Bifurcation diagrams for homogeneous shear flow with standard model parameters ($C_1 = 0.412$, $C_2 = 0.6$ and $C_\nu = 12.48$) and four different values of the dimensionless Rayleigh discriminant ϕ. For these parameter values, $\phi_- \simeq -0.049$ and $\phi_+ \simeq 0.243$. Solid and dotted lines indicate stable and unstable branches.

(*b*) $\phi_- < \phi < 0$. The turbulent branch bifurcates subcritically from the laminar state at the point of linear instability. There is an interval of Re in which stable laminar and turbulent solutions coexist.

(*c*) $0 < \phi < \phi_+$. The laminar state is linearly stable for all Re and the turbulent branch is disconnected from it. Only the upper turbulent branch is stable, but the unstable lower branch assists in diminishing the basin of attraction of the laminar state as Re is increased.

(*d*) $\phi_+ < \phi < \infty$. No turbulent solution exists and the laminar state is stable for all Re.

For non-rotating shear flows, or more generally, flows with zero angular-momentum gradient ($\phi = 0$), the laminar state is linearly stable for all finite values of Re. However, it is unstable with respect to algebraically growing disturbances at $Re = \infty$ and a branch of turbulent solutions bifurcates subcritically at this point (figure 2).

The conclusion of this analysis is that, according to our model, statistically steady and homogeneous turbulence can be sustained in a rotating uniform shear flow at sufficiently large Reynolds number provided that the flow is Rayleigh-unstable, Rayleigh-neutral or else Rayleigh-stable by a sufficiently small margin. For Rayleigh-neutral or slightly Rayleigh-stable flows the transition to turbulence occurs through a nonlinear instability of the laminar state, which has a diminishing basin of attraction as $Re \to \infty$. These properties are in accord with the generally accepted model of

https://doi.org/10.1017/S002211200500368X Published online by Cambridge University Press

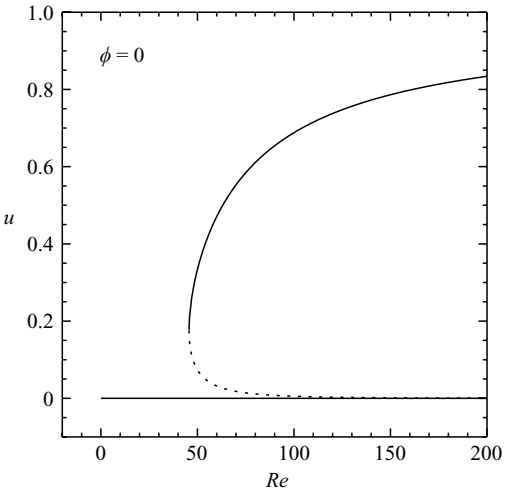


FIGURE 2. Bifurcation diagram for homogeneous shear flow with standard model parameters and vanishing Rayleigh discriminant, corresponding to a non-rotating shear flow. The branch of turbulent solutions bifurcates subcritically from the laminar state at $Re = \infty$.

transition to turbulence in shear flows (e.g. Grossmann 2000). Even though our model is designed principally to describe the statistical properties of fully developed turbulence, it appears to give a description of the onset of turbulence that is at least qualitatively reasonable.

Through straightforward algebra it can be shown that the turbulent solutions share the following properties:

(*a*) R_{ij} is positive definite and therefore the solutions are realizable;

(*b*) $\mathrm{sign}(-R_{xy}) = \mathrm{sign}(S)$ and therefore the turbulent transport of momentum has the same sense as viscous transport;

(*c*) $R_{xz} = R_{yz} = 0$ as expected on grounds of symmetry;

(*d*) the solutions are stable with respect to arbitrary perturbations of R_{xz} and R_{yz}.

In the limit $Re \to \infty$ equation (3.11) has at most one solution for which u tends to a positive limiting value. This solution exists when $\phi < \phi_+$, i.e. when the flow is Rayleigh-unstable, Rayleigh-neutral, or else Rayleigh-stable by a sufficiently small margin (Ogilvie 2003). In detail, the limiting solution is

$$\left.\begin{aligned} R_{xx} &= \left[\frac{3(1-Ro^{-1})C_1 + C_2}{C_1 + C_2}\right]\frac{R}{3}, \\ R_{xy} &= -\frac{C_1}{2LS}R^{3/2}, \\ R_{yy} &= \left(\frac{3Ro^{-1}C_1 + C_2}{C_1 + C_2}\right)\frac{R}{3}, \\ R_{zz} &= \left(\frac{C_2}{C_1 + C_2}\right)\frac{R}{3}, \end{aligned}\right\} \tag{3.13}$$

with

$$R = \left[\frac{C_2 - 6Ro^{-1}(Ro^{-1}-1)C_1}{C_1(C_1+C_2)^2}\right]\frac{2}{3}L^2S^2 = \frac{4(\phi_+ - \phi)}{(C_1+C_2)^2}L^2S^2. \tag{3.14}$$

For a fixed Rossby number satisfying the condition $\phi < \phi_+$, the turbulent momentum

https://doi.org/10.1017/S002211200500368X Published online by Cambridge University Press

transport has the dependence

$$-R_{xy} = \frac{4C_1}{(C_1+C_2)^3}(\phi_+ - \phi)^{3/2} L^2 S|S| \propto L^2 S|S|, \tag{3.15}$$

as also occurs in Prandtl's mixing-length theory. In our model, however, this result is obtained only in the limit of large Re, and the coefficient of proportionality depends on the Rossby number if the flow is rotating.

The turbulent states are always anisotropic owing to the effects of shear and rotation. In our model, the dimensionless anisotropy tensor

$$b_{ij} = \frac{R_{ij}}{R} - \frac{1}{3}\delta_{ij}, \tag{3.16}$$

which describes the shape of the Reynolds tensor, depends only on the ratio C_2/C_1 and on the Rossby number, when the Reynolds number is sufficiently large. When C_2/C_1 is small, the tendency to return to isotropy is weak and the stress becomes highly anisotropic. In principle, the ratio C_2/C_1 could be constrained through a comparison with experimental data on anisotropy. We return to this point in § 3.4 below.

3.2. *Turbulent shear flow past a wall*

In this section we analyse the simplest problem involving a wall-bounded turbulent shear flow. The solution will serve later as an asymptotic description of the turbulent boundary layers found in more complicated situations.

We consider the non-rotating parallel shear flow $\bar{\boldsymbol{u}} = \bar{u}_x(y)\,\boldsymbol{e}_x$ in the semi-infinite region $y > 0$ bounded by a smooth, stationary wall at $y = 0$ and forced by a shear stress $T_{xy} > 0$ at $y = \infty$. Even in a situation such as Couette–Taylor flow, it is usually permissible to neglect rotation in the turbulent boundary layers because the local shear rate is much larger than the rotation rate. Since the presence of the wall provides the only geometrical constraint on the turbulent structures, we set $L = y$, as is common in applications of mixing-length theory to wall-bounded flows. Indeed, throughout the remainder of this paper, we set L equal to the distance to the nearest wall.

We seek steady solutions of the averaged equations in which the mean quantities depend only on y, and with the expected symmetry property $R_{xz} = R_{yz} = 0$. The x-component of the averaged Navier–Stokes equation,

$$0 = \nu\partial_{yy}\bar{u}_x - \partial_y R_{xy}, \tag{3.17}$$

implies

$$\nu\partial_y\bar{u}_x - R_{xy} = T_{xy} = \text{constant}. \tag{3.18}$$

The non-trivial components of the Reynolds-stress equation in our model are

$$\left.\begin{aligned}
2R_{xy}\partial_y\bar{u}_x &= -\frac{(C_1+C_2)}{L}R^{1/2}R_{xx} + \frac{C_2}{3L}R^{3/2} + \nu\partial_{yy}R_{xx} - \frac{C_\nu\nu}{L^2}R_{xx},\\
R_{yy}\partial_y\bar{u}_x &= -\frac{(C_1+C_2)}{L}R^{1/2}R_{xy} + \nu\partial_{yy}R_{xy} - \frac{C_\nu\nu}{L^2}R_{xy},\\
0 &= -\frac{(C_1+C_2)}{L}R^{1/2}R_{yy} + \frac{C_2}{3L}R^{3/2} + \nu\partial_{yy}R_{yy} - \frac{C_\nu\nu}{L^2}R_{yy},\\
0 &= -\frac{(C_1+C_2)}{L}R^{1/2}R_{zz} + \frac{C_2}{3L}R^{3/2} + \nu\partial_{yy}R_{zz} - \frac{C_\nu\nu}{L^2}R_{zz},
\end{aligned}\right\} \tag{3.19}$$

subject to the no-slip boundary conditions $\bar{u}_x = R_{ij} = 0$ at $y = 0$.

https://doi.org/10.1017/S0022112005003680X Published online by Cambridge University Press

We rewrite the equations in a dimensionless form by means of the standard transformations

$$\bar{u}_x(y) = v(\eta)\sqrt{T_{xy}}, \qquad R_{ij}(y) = r_{ij}(\eta)T_{xy}, \qquad \eta = \frac{y\sqrt{T_{xy}}}{\nu}. \tag{3.20}$$

Observing the property $r_{zz} = r_{yy}$, which implies $r = r_{xx} + 2r_{yy}$, we obtain the reduced problem

$$v' - r_{xy} = 1, \tag{3.21}$$

$$\left.\begin{aligned} 2r_{xy}v' &= -\frac{(C_1+C_2)}{\eta}r^{1/2}r_{xx} + \frac{C_2}{3\eta}r^{3/2} + r''_{xx} - \frac{C_v}{\eta^2}r_{xx}, \\ r_{yy}v' &= -\frac{(C_1+C_2)}{\eta}r^{1/2}r_{xy} + r''_{xy} - \frac{C_v}{\eta^2}r_{xy}, \\ 0 &= -\frac{(C_1+C_2)}{\eta}r^{1/2}r_{yy} + \frac{C_2}{3\eta}r^{3/2} + r''_{yy} - \frac{C_v}{\eta^2}r_{yy}, \end{aligned}\right\} \tag{3.22}$$

with boundary conditions $v(0) = r_{ij}(0) = 0$.

The desired behaviour at $\eta = \infty$ can be deduced by analysing the far-field limit $\eta \gg 1$, for which we obtain the asymptotic form

$$\left.\begin{aligned} v' &\sim v'_1\eta^{-1} + v'_2\eta^{-2} + \cdots, \\ r_{ij} &\sim r_{ij0} + r_{ij1}\eta^{-1} + \cdots, \end{aligned}\right\} \tag{3.23}$$

with

$$v'_1 = \frac{C_1}{2}r_0^{3/2}, \qquad r_0 = \left(\frac{6}{C_1C_2}\right)^{1/2}(C_1+C_2), \tag{3.24}$$

$$r_{xx0} = \frac{(3C_1+C_2)}{3(C_1+C_2)}r_0, \qquad r_{xy0} = -1, \qquad r_{yy0} = \frac{C_2}{3(C_1+C_2)}r_0. \tag{3.25}$$

The reduced problem is universal, involving no parameters other than the model parameters C_1, C_2 and C_v. To solve it numerically, we use a finite-difference Newton–Raphson relaxation method on a stretched mesh, starting from an initial guess with $r_{ij} = r_{ij0}$ and $v = \eta$. The outer boundary condition $r'_{ij}(\eta_{\rm out}) = 0$, where $\eta_{\rm out} \gg 1$, imposes the desired far-field behaviour with adequate fidelity. We choose $\eta_{\rm out} = 10^5$. The desired universal boundary-layer solution is shown in figure 3. The stability of this solution has been confirmed using a time-dependent numerical method.

In the Prandtl–von Kármán analysis of turbulent boundary layers (e.g. Schlichting 1979) the velocity profile for $\eta \gg 1$ is given as

$$v \simeq A\ln\eta + B \tag{3.26}$$

where A and B are dimensionless empirical constants, and it is customary to refer to $\kappa = 1/A$ as the von Kármán constant. This 'universal velocity profile', 'log law' or 'law of the wall' is generally in excellent agreement with experimental data. The values traditionally assigned on the basis of Nikuradse's experiments in the 1930s are $\kappa = 0.41$ and $B = 5.2$ (for a smooth wall). However, recent experiments at higher Reynolds numbers show a much superior fit with $\kappa = 0.436$ and $B = 6.15$ (Zagarola & Smits 1998).

In our model the integrated velocity profile for $\eta \gg 1$ is

$$v(\eta) = v_0 + v'_1\ln\eta - \frac{v'_2}{\eta} + O(\eta^{-2}), \tag{3.27}$$

https://doi.org/10.1017/S002211200500368X Published online by Cambridge University Press

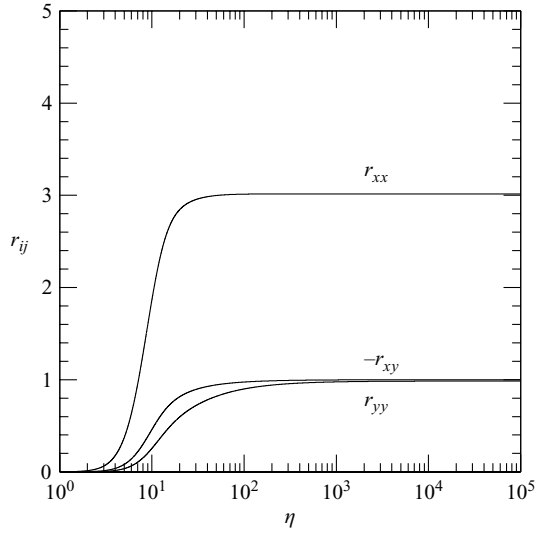


FIGURE 3. Universal boundary-layer solution for turbulent shear flow past a wall with standard model parameters. The dimensionless Reynolds stress components r_{xx}, $r_{yy} = r_{zz}$ and $-r_{xy}$ are shown.

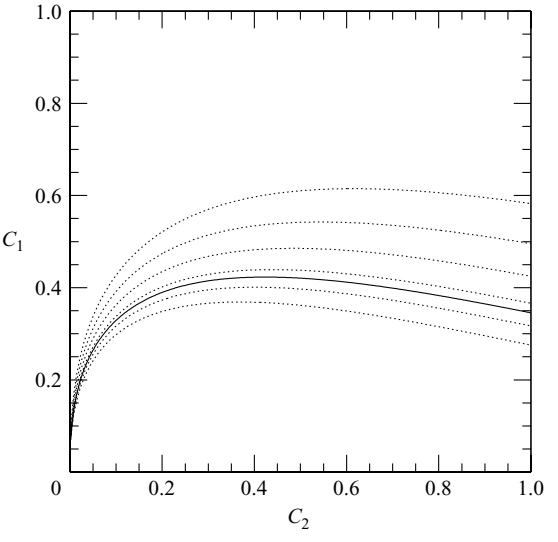


FIGURE 4. Contours of constant κ with (from bottom to top) $\kappa = 0.5$, 0.46, 0.436 (solid line), 0.42, 0.38, 0.34 and 0.3.

which is asymptotically equivalent to the Prandtl–von Kármán velocity profile; thus we identify the von Kármán constant as

$$\kappa = \frac{1}{v_1'} = \frac{2}{C_1}\left[\frac{C_1 C_2}{6(C_1 + C_2)^2}\right]^{3/4}. \tag{3.28}$$

The von Kármán constant depends only on C_1 and C_2 and can therefore be fitted independently of C_v. Figure 4 shows the relation between C_1 and C_2 for constant κ.

https://doi.org/10.1017/S002211200500368X Published online by Cambridge University Press

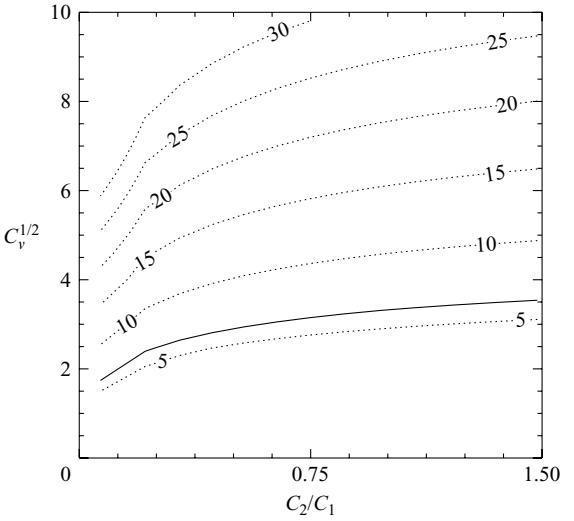


FIGURE 5. Contours of constant v_0 as a function of C_2/C_1 (for a fixed $\kappa = 0.436$) and $\sqrt{C_\nu}$. The solid line corresponds to the experimentally determined value of $v_0 = 6.15$. The uniform contour spacings suggest that v_0 depends primarily and approximately linearly on $\sqrt{C_\nu}$.

The additive constant $B = v_0$ cannot be deduced from the asymptotic analysis but must instead be determined from a numerical solution of the problem including the viscous sublayer close to the wall. Numerical integration of the boundary layer equations shows that v_0 depends primarily on C_ν, as shown in figure 5. For simplicity, in that figure we have reduced the parameter space by imposing the constraint $\kappa = 0.436$ (Zagarola & Smits 1998).

3.3. *Comparison with other models*

In comparison with other Reynolds-stress models available in the literature, our model appears quite simplistic (e.g. Speziale 1991). The viscous dissipation rate is given by

$$\epsilon = \frac{C_1}{2L} R^{3/2} + \frac{C_\nu \nu}{2L^2} R \tag{3.29}$$

and we do not attempt to model a separate time-dependent equation for this quantity. One reason for this is that the length scale L is imposed by the geometrical constraints in our problem, and is not free to expand as occurs when turbulence is generated in a localized region within a larger system. Instead, we allow for the effects of a finite Reynolds number by specifying a dissipation time scale that is related to the characteristic time scale $L/R^{1/2}$ of the largest eddies in high-Reynolds-number turbulence, and to the viscous time scale L^2/ν at lower Reynolds numbers.

In freely decaying turbulence with no mean shear or rotation, the return to isotropy is described in our model by the equation

$$\frac{\mathrm{d}b_{ij}}{\mathrm{d}\tau} = \frac{R}{\epsilon}\frac{\mathrm{d}b_{ij}}{\mathrm{d}t} = -\left(\frac{2C_2}{C_1 + C_\nu \nu L^{-1} R^{-1/2}}\right) b_{ij}, \tag{3.30}$$

where

$$b_{ij} = \frac{R_{ij}}{R} - \frac{1}{3}\delta_{ij} \tag{3.31}$$

https://doi.org/10.1017/S0022112005003680X Published online by Cambridge University Press

is the anisotropy tensor and τ is a dimensionless time variable (e.g. Speziale 1991). In the limit of large Reynolds number we therefore obtain a linear return to isotropy, equivalent to the one introduced first by Rotta (1951).

Furthermore, we do not attempt to model the 'rapid pressure–strain correlation', for which elaborate algebraic models have been proposed (e.g. Sjögren & Johansson 2000). Through this simplification we may lose some accuracy. However, it is the treatment of this term that has given rise to models that deal poorly with rotating shear flows. For example, the widely adopted model of Launder, Reece & Rodi (1975) is not consistent with Rayleigh's criterion in the sense that it does not permit turbulence to be sustained at high Reynolds number in certain situations where Rayleigh's stability criterion is not satisfied (Speziale 1991), perhaps because a realizability condition of some kind is implicitly violated. It is to be hoped that a way can be found to model the rapid pressure–strain correlation in future with due regard to Rayleigh's criterion.

3.4. *Summary of the constraints on the parameters C_1, C_2 and C_v*

We have purposely adopted a simple closure model for the Reynolds-stress equation so that we can focus on the nonlinear dynamical properties of the system rather than engaging in a lengthy exercise of parameter fitting. Nevertheless, because the model naturally predicts a logarithmic velocity profile close to a wall, it makes sense to apply the two accurate constraints $\kappa = 0.436$ and $v_0 = 6.15$ provided by the very high-quality experimental data on wall-bounded turbulent shear flows in the Superpipe experiment (Zagarola & Smits 1998). The first constraint provides a relation between C_1 and C_2 only, whereas the second (which applies only for a smooth wall) yields C_v provided that C_1 and C_2 are known. A third constraint, which would be required to fix all three parameters of our model, might in principle be provided by experimental data on the anisotropy of the Reynolds stress in homogeneous shear turbulence, or on the return to isotropy of homogeneous turbulence. In fact, the limitations of the three-parameter model mean that no choice of the parameters can accurately match all experimental results. For example, Choi & Lumley (2001) find that the return to isotropy of homogeneous turbulence is more complicated than is assumed in any available closure model. In § 4.2 below we compare the predictions of our model with data from Couette–Taylor experiments, and tentatively deduce an approximate value of $C_2 \simeq 0.6$. Hence in what follows (unless otherwise mentioned) we shall take as standard parameters $C_1 = 0.412$, $C_2 = 0.6$ and $C_v = 12.48$, which yield $\kappa = 0.436$ and $v_0 = 6.15$ as required. The predicted boundary-layer velocity profile with this choice of parameters is compared with the experimental measurements of Zagarola & Smits (1998) in figure 6.

4. Couette–Taylor flow

Couette–Taylor flow between differentially rotating coaxial cylinders is a seemingly simple dynamical system that has been found to exhibit a rich variety of nonlinear behaviour. Much of this interesting dynamics occurs close to the onset of Rayleigh's centrifugal instability, albeit in a confined setting and in the presence of viscosity. Our main interest here is in the existence and properties of turbulent states in Couette–Taylor flow at large Reynolds numbers, rather than the behaviour close to the onset of instability. This aspect of the problem has received rather little attention from experimentalists or turbulence modellers. Recently, however, arguments based on the Couette–Taylor system have been made in connection with important

https://doi.org/10.1017/S002211200500368X Published online by Cambridge University Press

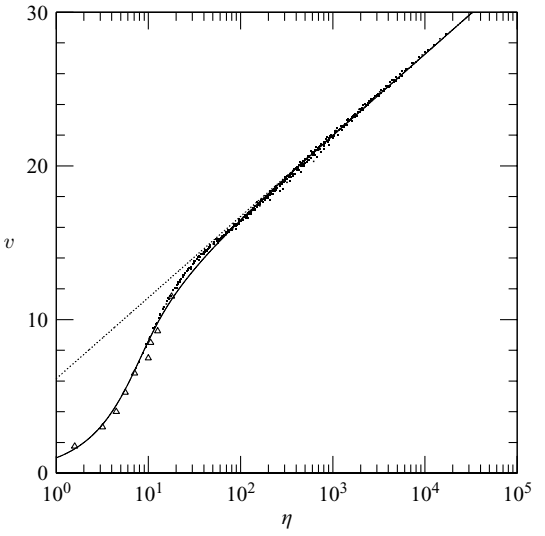


FIGURE 6. Solution of the dimensionless boundary-layer problem for turbulent shear flow past a wall with standard model parameters. The dotted line corresponds to the asymptotic profile $v = (0.436)^{-1} \ln \eta + 0.615$ (Zagarola & Smits 1998) which is their suggested best fit for their experimental results. The small black dots are the experimental data points from Zagarola & Smits, corrected for systematic errors according to the prescriptions of McKeon *et al.* (2003). The open triangles are the experimental data points from Reichardt (1940).

questions relating to turbulence in astrophysical flows involving differential rotation (e.g. Richard & Zahn 1999).

Since our Reynolds-stress model is based on a covariant formulation, it naturally includes the effect of rotation as well as shear. In this section we apply the model to the Couette–Taylor system, compare its predictions with the available experimental results and examine the wider consequences of these findings.

4.1. *Predictions of the model*

4.1.1. *Governing equations and numerical solution*

We consider the shear flow between two infinite coaxial cylinders located at radii r_i and r_o, rotating with angular velocities Ω_i and Ω_o. Adopting a cylindrical coordinate system (r, ϕ, z), we seek steady solutions of the averaged equations in which the mean quantities depend only on r and the mean flow is azimuthal only: $\bar{\boldsymbol{u}} = r\Omega(r)\,\boldsymbol{e}_\phi$. In this case the Reynolds-stress equation in our model reduces to (A 6) and straightforward algebra yields $R_{rz} = R_{\phi z} = 0$. We choose the scale length L to be the distance to the nearest wall, namely $L = \min(r - r_i, r_o - r)$.

Experiments on Couette–Taylor flow, using a cylindrical container of finite height h, are perturbed by end effects, in particular the Ekman circulation, when the aspect ratio $h/(r_o - r_i)$ is not very large. We do not attempt to model end effects, but note their potential significance when comparing our findings with experimental results (see § 4.2.1).

The angular velocity profile $\Omega(r)$ between the cylinders is obtained self-consistently by solving also the angular momentum conservation equation (the azimuthal component of the averaged Navier–Stokes equation),

$$\frac{\mathrm{d}}{\mathrm{d}r}(r^2 R_{r\phi} + \nu r^2 S) = 0 \tag{4.1}$$

https://doi.org/10.1017/S002211200500368X Published online by Cambridge University Press

where $S = -r\,\mathrm{d}\Omega/\mathrm{d}r$ is the shear rate in cylindrical geometry. Note that equation (4.1) can be integrated to introduce the torque T between the cylinders,

$$r^2 R_{r\phi} + \nu r^2 S = \frac{T}{2\pi h \rho}. \tag{4.2}$$

We obtain a ninth-order system of ODEs with one eigenvalue (T) which requires ten boundary conditions: $R_{rr} = R_{r\phi} = R_{\phi\phi} = R_{zz} = 0$ on each boundary, as well as $\Omega(r_i) = \Omega_i$ and $\Omega(r_o) = \Omega_o$. We solve this two-point boundary-value problem numerically using a Newton–Raphson relaxation method, using the solution for $Re \to \infty$ as an initial guess (or, whenever applicable, the results of a previous calculation for similar parameters).

In addition to possible turbulent solutions, there is of course the well-known laminar Couette–Taylor flow $\Omega(r) = \alpha + \beta/r^2$, where $\alpha = (\Omega_o r_o^2 - \Omega_i r_i^2)(r_o^2 - r_i^2)^{-1}$ and $\beta = (\Omega_i - \Omega_o) r_i^2 r_o^2 (r_o^2 - r_i^2)^{-1}$. The local dimensionless Rayleigh discriminant of the laminar solution is $\phi(r) = (\alpha/\beta)^2 r^4 + (\alpha/\beta) r^2$. Unlike plane Couette flow, the laminar Couette–Taylor flow is linearly unstable in certain regions of the parameter space. Therefore turbulent states may be accessed through either linear or nonlinear instabilities.

4.1.2. *Asymptotic analysis*

The results presented in § 3.2 suggest that the system of equations (A 6) and (4.2) could also be solved approximately by asymptotic matching, between the universal boundary-layer solution near the wall and a high-Reynolds-number limiting solution ($Re \to \infty$) in the main body of the fluid. When $Re \to \infty$, the turbulent solution is

$$R = \left[\frac{C_2 - 6Ro^{-1}(Ro^{-1} - 1)C_1}{C_1(C_1 + C_2)^2}\right] \frac{2}{3} L^2 S^2, \tag{4.3}$$

whenever this is positive, and then

$$R_{r\phi} = \frac{C_1}{2LS} R^{3/2} = \frac{C_1}{2} \left(\frac{2}{3}\right)^{3/2} \left[\frac{C_2 - 6C_1 Ro^{-1}(Ro^{-1} - 1)}{C_1(C_1 + C_2)^2}\right]^{3/2} L^2 S|S|, \tag{4.4}$$

by direct analogy with results (3.14) and (3.15) of the local analysis. Unfortunately, there exist no analytical solutions to the angular momentum equation with this Reynolds stress prescription unless $Ro \gg 1$. The Rossby number of the laminar flow is large for typical narrow-gap setups; one might therefore hope to use this asymptotic limit for the study of the turbulent regime also. However, numerical solution of equations (A 6) and (4.2) reveals that turbulence effectively reduces the shear outside the boundary layers and prevents the use of the $Ro \gg 1$ asymptotic limit unless the gap is extremely small (typically, less than a few percent of the average radius). For completeness, we nevertheless provide such an asymptotic analysis in Appendix B.

4.1.3. *Stability diagram and structure of solutions across parameter space*

In what follows, we call the Couette–Taylor flow 'unstable' whenever there exist solutions to the equations of the model with $R > 0$. By doing so, we implicitly assume that the background noise level is sufficiently high to excite finite-amplitude instabilities if they exist. Figure 7 shows a stability diagram for corotating cylinders in the (Re_o, Re_i) plane (where $Re_o = d r_o \Omega_o/\nu$ and $Re_i = d r_i \Omega_i/\nu$, with $d = r_o - r_i$) for a given geometrical setup ($r_i/r_o = 0.7$). As predicted by the local analysis, Rayleigh-stable flows can be subject to finite-amplitude instabilities provided they are notionally Rayleigh-stable by a small margin only, thus displacing the stability boundary in

https://doi.org/10.1017/S002211200500368X Published online by Cambridge University Press

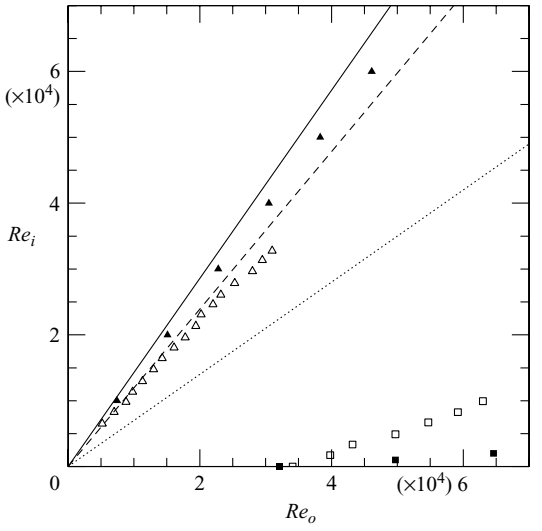


FIGURE 7. Stability boundaries for Couette–Taylor flow in a fixed geometrical setup ($r_i/r_o = 0.7$), predicted with standard model parameters. The black symbols are the predictions of our model, and delimit the regions of turbulent solutions in the top-left and bottom-right corners. The open symbols are the data from Richard (2001) for the same geometrical setup. The solid line is the stability limit according to Rayleigh's criterion ($\Omega_i r_i^2 = \Omega_o r_o^2$), the dashed line marks the Keplerian ratio ($\Omega_i r_i^{3/2} = \Omega_o r_o^{3/2}$) and the dotted line marks solid-body rotation ($\Omega_i = \Omega_o$).

the top-left corner of the diagram by a small amount. Strong enough shear can overcome the stabilizing angular-momentum gradient in the case where $Re_o \gg Re_i$ and finite-amplitude instabilities are also found in that region (bottom-right corner of the diagram). The predicted onset of instability in the case of relatively low Reynolds numbers and also of counter-rotating cylinders is discussed further in § 4.2.3. Comparison with experimental data from Richard *et al.* (2001) shows significant discrepancies with the predictions of the model, though this could be expected because the aspect ratio of their experimental setup is not large (see the discussion in § 4.2.1).

The structure of the solutions in various regions of parameter space, as shown in figure 8, reflects the physics of turbulent flow. In the case where the outer cylinder is at rest, the local dimensionless Rayleigh discriminant for the laminar solution is

$$\phi(r) = (r/r_o)^4 - (r/r_o)^2 \tag{4.5}$$

and is therefore always negative (Rayleigh-unstable). Viscosity stabilizes the flow for sufficiently low Reynolds number Re_i but the transition to turbulence occurs directly, through a linear instability (the critical value for the transition depends on the geometrical setup). Turbulent stresses are largest in the bulk of the fluid, near the mid-point $r_m = (r_o + r_i)/2$.

In the case where the inner cylinder is at rest,

$$\phi(r) = (r/r_i)^4 - (r/r_i)^2 \tag{4.6}$$

is always positive (Rayleigh-stable). Linear instability is therefore not expected, but turbulent states may still be accessed through a nonlinear instability. Sufficiently close to the inner cylinder, in the region where $\phi < \phi_+$, the local analysis would suggest that

https://doi.org/10.1017/S002211200500368X Published online by Cambridge University Press

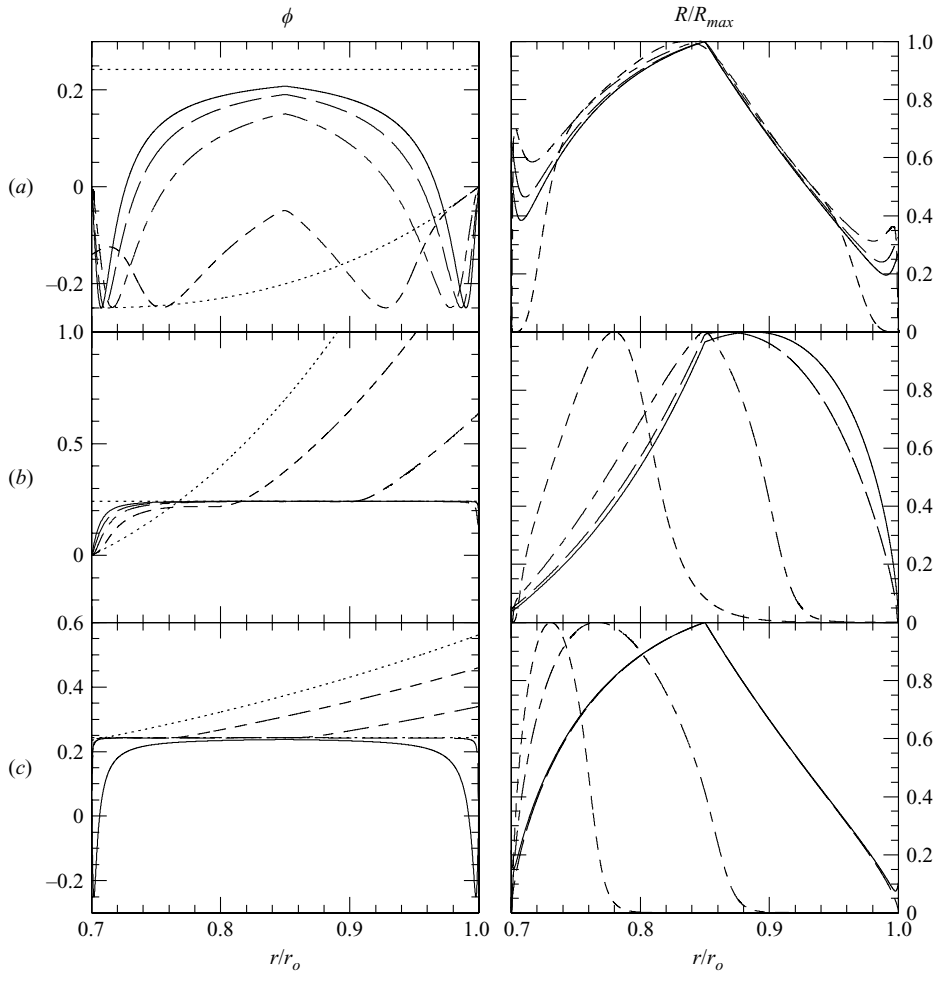


FIGURE 8. Structure of solutions for a fixed geometrical setup with $r_i/r_o = 0.7$, for three regions of parameter space in the case of corotating cylinders. The left-hand column shows the local dimensionless Rayleigh discriminant $\phi(r)$; in each figure, the horizontal dotted line marks the position of the critical value $\phi_+ = C_2/6C_1 \simeq 0.243$. The right-hand column shows the mean-square turbulent velocity, normalized to its maximum value for clarity. The top two panels (*a*) correspond to the case where the outer cylinder is at rest, with the laminar solution marked as a dotted line, then the outer cylinder rotation rate is steadily increased with $Re_o = 10^3$ (dashed line), $Re_o = 10^5$ (short-long dashed line), $Re_o = 10^7$ (long-dashed line) and $Re_o = 10^9$ (solid line). The line-style coding is the same for both plots. Panels (*b*) correspond to the case when the inner cylinder is at rest, showing the laminar solution (dotted line), then turbulent solutions for $Re_o = 10^5$ (dashed line), $Re_o = 10^6$ (short-long-dashed line), $Re_o = 10^7$ (long-dashed line) and $Re_o = 10^9$ (solid line). Panels (*c*) correspond to the onset of instability near the Rayleigh stability limit. The outer cylinder rotation is fixed ($Re_o = 10^9$) and the inner cylinder rotation is varied. The solution is laminar (dotted line) for $Re_i = 1.22 \times 10^9$, then becomes successively more turbulent for $Re_i = 1.24 \times 10^9$ (dashed line), $Re_i = 1.26 \times 10^9$ (short-long-dashed line) and $Re_i = 1.28 \times 10^9$ (long-dashed line). The last curve lies further away from onset, and into the Rayleigh-unstable zone with $Re_i = 2 \times 10^9$ (solid line).

the laminar solution is unstable to finite-amplitude perturbations provided the local Reynolds number is large enough. Depending on the gap width, two situations may arise: either $0 < \phi < \phi_+$ for all r, or there exists a transition within the fluid between

https://doi.org/10.1017/S002211200500368X Published online by Cambridge University Press

a locally stable region and a region of finite-amplitude instability. An equivalent way of looking at the problem is to note that the stabilizing effect of rotation on the development of turbulence is weaker near the inner boundary when the inner cylinder is at rest, and so we expect turbulence to develop first near the inner cylinder (as can indeed be seen in figure 8).

Finally, we explore the behaviour of solutions near the onset of nonlinear instability at very high Reynolds number in the region close to the Rayleigh line ($\Omega_i r_i^2 = \Omega_o r_o^2$). The transition to turbulence occurs when ϕ for the laminar solution near the inner cylinder drops below ϕ_+. This happens in the Rayleigh-stable domain. As Re_i is increased, ϕ on the outer cylinder drops below 0 which marks the transition to the Rayleigh-unstable domain.

The structure of the solutions in all three cases seems to suggest that turbulence is extremely efficient in transporting the applied torque: the marginal solution $\phi = \phi_+$ is favoured near onset and also in the Rayleigh-stable case far from onset. In the latter case the solution deviates from the marginal stability solution only in the thin viscous boundary layers. This behaviour is typically also observed in convection. In the Rayleigh-unstable case on the other hand, a solution with $\phi = \phi_+ > 0$ could not possibly satisfy the applied boundary conditions, and the flow appears to compromise by choosing an intermediate solution with $\phi < 0$ in a significant part of the domain.

4.2. *Comparison with experimental data*

4.2.1. *Discussion of available data*

Since Taylor's (1923) pioneering work on the stability of fluid flows between two coaxial rotating cylinders, a wealth of experimental data has been collected on the dynamical properties of such flows for various aspect parameters (r_i, r_o, h) and for a very large region of the (Re_o, Re_i) parameter space. In particular, Wendt (1933) and Taylor (1936*a*, *b*) presented the most extensive collection of torques and velocity measurements for turbulent Couette–Taylor flow far from onset, whereas Andereck, Liu & Swinney (1986) reviewed the successive flow-pattern transitions near onset.

Amongst other notable results, Wendt (1933) studied the contaminating Ekman flows arising from end effects, which can drive significant deviations from the laminar Couette–Taylor flow. He proposed an ingenious system including a free top surface and a differentially rotating split bottom plate to reduce end effects; this setup is indeed able to reduce meridional flows but not completely. Comparisons of torque measurements between various bottom boundary conditions revealed that end effects are especially important for aspect ratios h/d smaller than 40. Wendt performed experiments with only the outer cylinder rotating, and showed that torque measurements made with bottom plates corotating with the outer cylinder were roughly 10% larger than in the case where the bottom plates are stationary for an aspect ratio of 50, 100% larger for an aspect ratio 23 and 400% larger for an aspect ratio of 11. Naturally, any theory that assumes axial translational symmetry for the system (as does the model investigated here) can only be compared with experiments that have little contamination from end effects, and we may use Wendt's findings as a guideline for distinguishing between adequate and inadequate sets of experiments.

Experiments at very high Reynolds number, and with a wide gap ($r_i/r_o = 0.724$), have been performed in the case where only the inner cylinder is rotating by Lathrop, Fineberg & Swinney (1992) and more recently by Lewis & Swinney (1999). Richard *et al.* (2001) have performed such experiments ($r_i/r_o = 0.7$) with both inner and outer cylinders rotating, using split-bottom boundary conditions. Wide-gap setups are well suited to verify the adequacy of our theory in describing the effects of rotation

https://doi.org/10.1017/S002211200500368X Published online by Cambridge University Press

on turbulent shear flows (as opposed to narrow-gap setups, which are principally dominated by the shear instability). However, all these experiments have too small ($\leqslant 25$) an aspect ratio to be free of end effects, so we cannot use them reliably for comparison with our work.

In what follows (§ 4.2.2), we first compare the predictions of our model with the torque measurements from Wendt (1933) in order to obtain a third constraint on our parameters C_1, C_2 and C_ν, as anticipated in § 3.4. We then compare the model to Taylor's (1936*a*) data. In § 4.2.3 we look at the predictions of the model for the onset of linear instability in Couette–Taylor flows and compare it with Taylor's (1923) experimental work. Finally, we discuss the stability of Keplerian shear flows in the light of our model, and compare our predictions with those of Richard & Zahn (1999) in § 4.2.4.

4.2.2. *Torque measurements*

Wendt's (1933) torque measurements present the most extensive results for an experimental setup with large aspect ratio. By using his narrow-gap data, which are relatively free from contaminating end effects, we attempt to constrain our basic parameters further. Wendt presents the results of twelve sets of experiments for the following setup: $h = 50\,\mathrm{cm}$, $r_o = 14.70\,\mathrm{cm}$ and $r_i = 13.75\,\mathrm{cm}$. For each set of measurements, the ratio of the rotation rates of the inner and outer cylinders is fixed, and the Reynolds number† is defined as

$$Re = \frac{|\Omega_o - \Omega_i| r_m d}{\nu}. \tag{4.7}$$

Wendt plots in his figure 9(*c*) the ratio of the turbulent to the laminar torque. We have performed ten suites of numerical calculations where C_2 is varied between 0.1 and 1 by increments of 0.1, and for each set have calculated the typical error between the predictions of our model and Wendt's experimental data points with the formula

$$E(C_2) = \sum \left[\left.\frac{T}{T_{\mathrm{lam}}}\right|_{\mathrm{mod}} - \left.\frac{T}{T_{\mathrm{lam}}}\right|_{\mathrm{exp}} \right]^2, \tag{4.8}$$

where the sum spans all data points in all twelve sets of experiments. The results are shown in figure 9 and suggest that the best fit is obtained with parameters $C_1 = 0.412$, $C_2 = 0.6$ and $C_\nu = 12.48$, which we have adopted as standard throughout this paper. The corresponding fit to Wendt's experimental data is shown in figure 10. We note that the fit is quite good though we are not able to fit all the curves equally well. In particular, the experimental results for a stationary inner cylinder (black circles on the right-hand panel) seem to deviate significantly from the predictions of our model for all possible values of C_2. Leaving this particular set of experiments out of the least-square fitting procedure seems to reduce the optimal value of C_2, but not significantly (see the square symbols in figure 9, which have a minimum near $C_2 = 0.55$). We emphasize that the constraint on our parameters obtained by fitting Wendt's data is much less satisfactory than the two tight constraints provided by the universal velocity profile of turbulent boundary layers. Therefore the estimate $C_2 = 0.6$ is to be regarded as tentative and approximate only.

We then tested the predictions of the model against Taylor's (1936*a*) torque measurements. Taylor's data consist of eight sets of experiments for varying gap

† Wendt actually uses a quantity related to the Reynolds number, $(60/2\pi)|\Omega_o - \Omega_i|/\nu$.

https://doi.org/10.1017/S002211200500368X Published online by Cambridge University Press

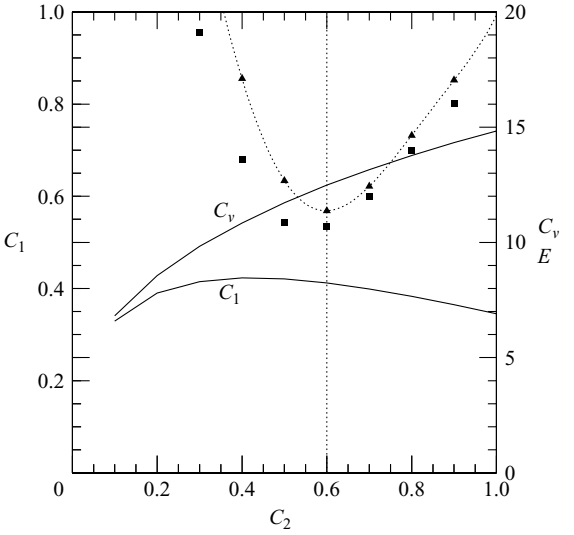


FIGURE 9. Study of the model parameters that best fit Wendt's (1933) experimental data. For each value of C_2, C_1 is chosen such that $\kappa = 0.436$ and C_v is chosen such that $v_0 = 6.15$. The corresponding values of C_1 and C_v are shown as solid lines, with the relevant scales on the left and right of the plot respectively. Using these parameters, the error E (as given by equation (4.8)) is calculated and shown as triangular symbols. The minimum error occurs for $C_2 = 0.6$. We also plot the error E calculated when leaving out the experimental results for stationary inner cylinder as square symbols.

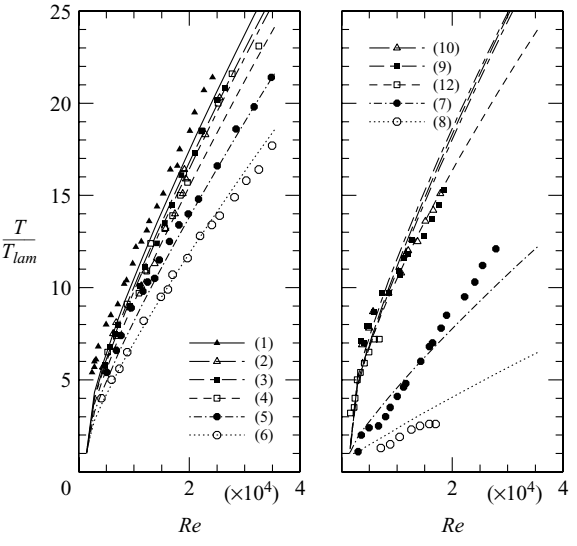


FIGURE 10. Comparison between the predictions of the model for $C_1 = 0.412$, $C_2 = 0.6$ and $C_v = 12.48$ and Wendt's (1933) data extracted from his article, figure 9(c). Panel (a) corresponds to his measurements for counter-rotating cylinders, and (b) corresponds to corotating cylinders. The corresponding line-styles and symbols are shown in each diagram, and the numbers in brackets refer to the original numbering used by Wendt (1933) to label his experiments.

https://doi.org/10.1017/S002211200500368X Published online by Cambridge University Press

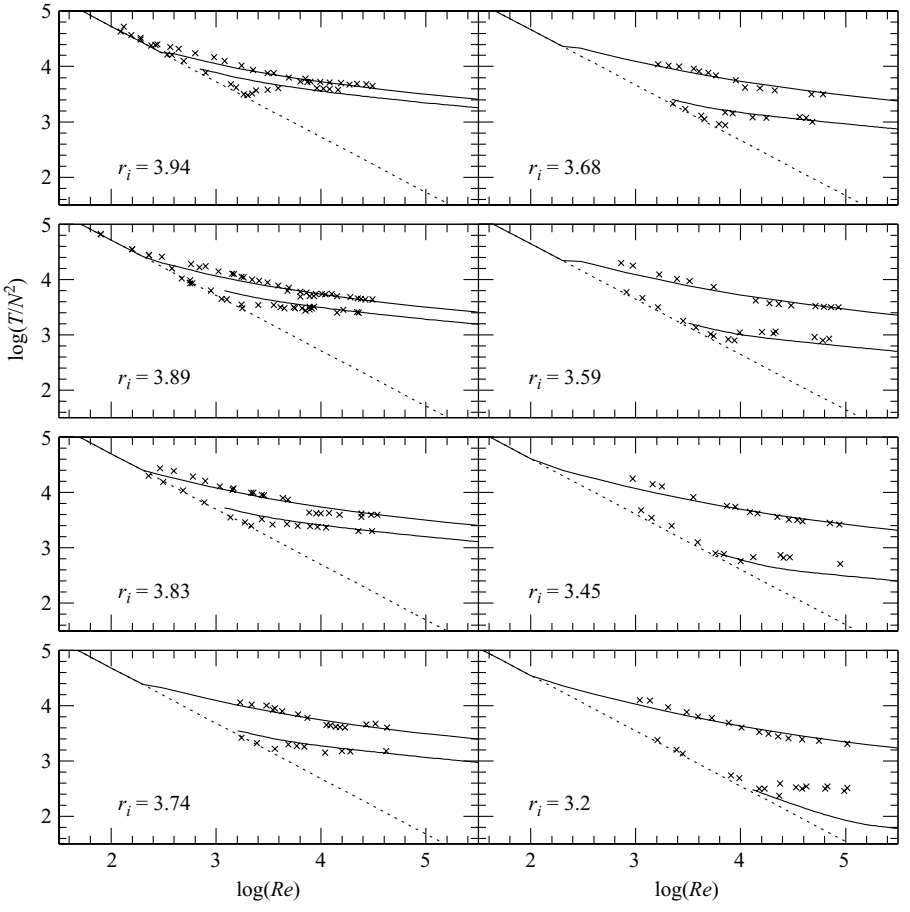


FIGURE 11. Comparison between Taylor's original data (1936*a*) and the predictions of our model with standard parameters. For each panel, the outer cylinder has radius $r_o = 4.05\,\text{cm}$ and the inner cylinder radius r_i is given in cm. The upper branch corresponds to the torques measured on the outer cylinder when the inner cylinder is rotating, and the lower branch corresponds to torques measured on the inner cylinder when the outer cylinder is rotating. The angular rotation rate Ω is related to N as $\Omega = 2\pi N$. The dotted line shows the laminar solution whereas the solid line is the prediction of the model. The quantity T/N^2 is measured in CGS units.

width; he compares the torques measured for similar Reynolds numbers† (as defined by equation (4.7)) when only the inner cylinder is rotating, and when only the outer cylinder is rotating. The results are presented in figure 11; the predictions of the model show excellent agreement with the experimental data, even near onset, in the case where only the inner cylinder is rotating. The agreement is also very good (except for the two widest gap widths) in the case where only the outer cylinder is rotating, except near onset. However, Taylor reports that the onset of instability in the case where only the outer cylinder is rotating undergoes hysteresis (where the turbulent solution can only be accessed through finite-amplitude perturbations); since our model assumes that the turbulent solution is chosen whenever it exists, we

† Taylor actually uses a quantity related to the Reynolds number, $\Omega/2\pi\nu$.

https://doi.org/10.1017/S002211200500368X Published online by Cambridge University Press

represent only the turbulent branch of the hysteresis loop, whereas it appears that Taylor's data follows the laminar branch up to a critical Reynolds number that may depend on the amount of noise present in his apparatus (see Schultz-Grunow 1959 for an assessment of the critical Reynolds number for the persistence of laminar flow in a noise-free Couette–Taylor system).

4.2.3. *Onset of instability in Couette–Taylor flows*

Although our model was initially designed for fully developed turbulent flows at very high Reynolds number, and in fact in the context of astrophysical magnetohydrodynamics (Ogilvie 2003), we now show that the addition of the viscous correction terms (see § 2) is also able to reproduce (qualitatively, and to some extent also quantitatively) the onset of instability in the Couette–Taylor system.

The classic work of Taylor (1923) combined experimental and theoretical studies of the onset of linear instability in the laminar Couette–Taylor flow for both corotating and counter-rotating cylinders. Impressive agreement was found between the appearance of axisymmetric Taylor vortices in the experiments and the occurrence of an axisymmetric linear instability in the theoretical calculation. We have investigated the linear stability of the laminar flow within the context of our model. To do this, we linearize the Reynolds-stress equation about the laminar solution and seek solutions of the form $R_{ij} = \tilde{R}_{ij}(r)\,\mathrm{e}^{st}$. The linearized system of ordinary differential equations admits a set of discrete modes, with the growth rate s appearing as an eigenvalue. We solve this system numerically and identify the stability boundary as the position in the parameter space where the largest eigenvalue passes through zero. The results depend on C_v, but not on C_1 or C_2 as these two parameters appear only in nonlinear terms.

The linear stability boundary predicted by our model is shown in figure 12 in comparison with Taylor's experimental results. For $C_v = 12.48$ the agreement is quite good (an even better fit can be obtained for $C_v = 11$). We therefore again find that, although our model is designed principally to describe fully developed turbulence, it also performs quite well in describing the onset of instability. Of course, Taylor vortices themselves are not a turbulent flow, but our model does not make a clear distinction between coherent and turbulent flows at relatively low Reynolds numbers. The near coincidence between our linear stability results and Taylor's is not trivial because, unlike him, we do not represent or solve for the optimal axial wavenumber of the linear disturbance.

Also shown in figure 12 is the nonlinear stability boundary which delimits the region of parameter space in which our model predicts turbulent solutions to exist. The discrepancy with Taylor's results illustrates the fact that a finite-amplitude instability, apparently not detected in Taylor's (1923) experiments, may occur in the case of counter-rotating cylinders. This idea is supported by the results of Coles (1965), who reports on the existence of a well-defined hysteresis zone delimited by a boundary qualitatively similar to our nonlinear stability boundary.

This boundary turns over and crosses the $Re_i = 0$ axis for finite Re_o. The unstable domain thus delimited for $Re_i < 0$, $Re_o < 0$ is the point-symmetric domain to the one identified as a region of finite-amplitude shear instability in the quadrant $Re_i > 0$, $Re_o > 0$ (see § 4.1.3 and figure 7).

4.2.4. *Keplerian shear flows*

An important unsolved problem in astrophysics concerns the hydrodynamic stability of accretion disks in which gas flows in circular Keplerian orbits with

https://doi.org/10.1017/S002211200500368X Published online by Cambridge University Press

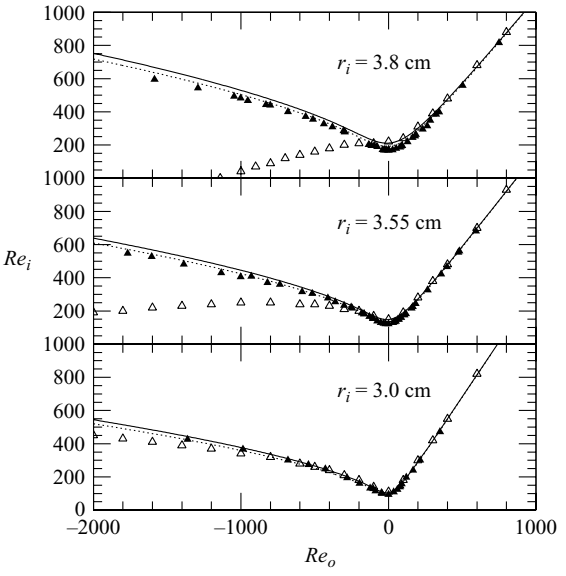


FIGURE 12. Comparison between the predictions of our model for linear and nonlinear stability of Couette–Taylor flow between two cylinders with $r_o = 4.035\,\text{cm}$ and r_i as shown in the plots, and Taylor's (1923) experimental data for the onset of instability. The black symbols correspond to Taylor's data, the open symbols corresponds to the onset of nonlinear instability as calculated with our full model for standard parameters. The solid line corresponds to the onset of instability calculated through a linear stability analysis of our turbulent model for $C_v = 12.48$ and the dotted lines show the same thing for $C_v = 11$.

$\Omega \propto r^{-3/2}$. Although magnetohydrodynamic instabilities are known to be effective in generating turbulent motion and angular momentum transport in disks that are sufficiently ionized (e.g. Balbus & Hawley 1998), such mechanisms probably fail to operate in some important circumstances such as in very weakly ionized regions of protoplanetary disks.

Recently, Richard & Zahn (1999) suggested, not unreasonably, that the stability of Keplerian flows might be deduced from the results of wide-gap Couette–Taylor experiments. They extract from Taylor's (1936*a*) and Wendt's (1933) data that the critical Reynolds number for instability, in the case where the inner cylinder is at rest, varies roughly as d^2/r_m^2 for wide gaps. From this result they deduce that there must exist a local Reynolds number for rotating shear flows

$$Re_{RZ} = \frac{r^3}{\nu}\left|\frac{\partial \Omega}{\partial r}\right| \tag{4.9}$$

with a critical value $Re_{c,RZ} \simeq 6.3 \times 10^5$ for instability (see figure 13). If such an abstraction of the Couette–Taylor experiments to Keplerian flows is indeed justified, this criterion would suggest that Keplerian disks (which typically have Reynolds numbers many orders of magnitude larger than this critical value) are indeed likely to be turbulent. Numerical solutions of our model near the onset of nonlinear instability in the case where the inner cylinder is at rest also reveal that the critical Reynolds number for instability varies as d^2/r_m^2 for wide gaps, although the proportionality constant is lower (see figure 13). The same argument proposed by Richard & Zahn (1999) applied to our results would therefore also suggest that Keplerian shear flows

https://doi.org/10.1017/S002211200500368X Published online by Cambridge University Press

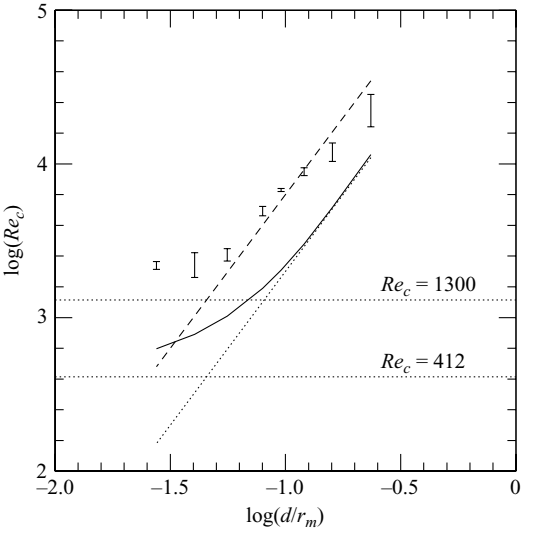


FIGURE 13. Critical Reynolds number $Re_c = \min(Re_o)$ for the onset of nonlinear instability in the case where the inner cylinder is at rest, as a function of gap width ($r_o = 4.05\,\mathrm{cm}$ for all points, and r_i is varied between 3.2 cm and 3.94 cm). The error bars reproduce Taylor's own interpretation of his data (1936*a*) with the size of the error bar corresponding to the extent of the hysteresis loop. The dashed line is the fit proposed by Richard & Zahn (1999), with $Re_c = 6.3 \times 10^5 (d/r_m)^2$; the solid line is our own results, and the inclined dotted line is a fit for the wide-gap limit with $Re_c = 2 \times 10^5 (d/r_m)^2$. The two horizontal lines are critical Reynolds numbers for plane Couette flow: $Re_c = 1300$ is derived from Dauchot & Daviaud's (1995) experiments, and $Re_c = 412$ is the prediction of our model.

should be unstable. However, a local analysis of our model predicts instability for Keplerian shear flows in the limit of large Reynolds numbers only when $C_2/C_1 > 8/3$ (Ogilvie 2003), which is not the case for the standard model parameters chosen in this numerical experiment. Hence, it is not clear that a generalization between Couette–Taylor results with a stationary inner cylinder and Keplerian flows can be made.

More generally, it is not clear that stability results for wall-bounded flows can be applied to unbounded flows. The instability may be triggered precisely by the presence of the boundaries (both the side walls, through the non-local effect of a redistribution of the shear profile between the cylinders, and the bottom boundary, through contaminating Ekman flows). For instance, in figure 14 we explore the stability of Couette–Taylor systems with inner and outer cylinders in Keplerian ratios ($\Omega_i r_i^{3/2} = \Omega_o r_o^{3/2}$). As mentioned earlier, if walls were absent and the shear was everywhere Keplerian, the local analysis of our model would only predict instability if $C_2/C_1 > 8/3$. However, we find that for large enough Reynolds numbers, instability can be found for ratios of $C_2/C_1 < 8/3$ in a wall-bounded experiment. This behaviour is possible because the dimensionless Rayleigh discriminant ϕ of the laminar solution is not uniform.

5. Discussion

In this paper we have investigated the nonlinear dynamics of turbulent shear flows, with and without rotation, in the context of a simple but physically motivated

https://doi.org/10.1017/S002211200500368X Published online by Cambridge University Press

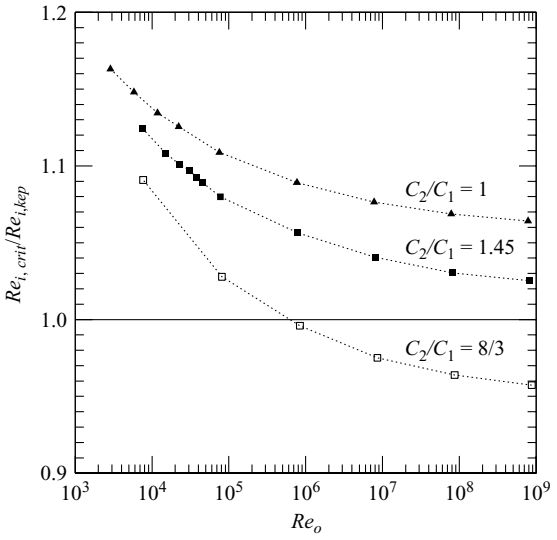


FIGURE 14. Predictions of the model for the onset of instability in a Couette–Taylor system identical to that of Richard (2001) with $r_o = 5\,\text{cm}$, $r_i = 3.5\,\text{cm}$. For each outer cylinder rotation rate (represented by its Reynolds number Re_o), the curves represent the ratio of the critical Reynolds number $Re_{i,crit}$ for instability to the Reynolds number corresponding to a Keplerian rotation rate for the inner cylinder $Re_{i,kep} = Re_o(r_o/r_i)^{1/2}$.

closure of the equation governing the evolution of the Reynolds stress tensor. In order to permit a detailed exploration of the nonlinear behaviour and to emphasize the physical interpretation of the dynamics, the approach we have taken differs from that of the conventional closure models used in engineering applications. We have not developed a model of great algebraic sophistication and attempted to fit the large number of parameters therein by applying a restricted class of constraints. Instead, we have adopted a minimal closure of the Reynolds-stress equation in which the modelled nonlinear terms have a clear interpretation and are as few in number as is compatible with the physical requirements.

Our model, equation (2.9), retains the exact form of the linear terms representing the advection of the turbulent fluctuations by the mean flow, their interaction with the mean velocity gradient and the viscous diffusion of the Reynolds stress, while using a minimal set of algebraic terms with three dimensionless parameters to represent dissipation through a turbulent cascade (with parameter C_1) and through direct viscous damping (parameter C_ν), as well as the tendency to return to isotropy (parameter C_2).

In a local analysis of homogeneous shear turbulence with or without rotation (§ 3.1), our closure model reduces to an autonomous nonlinear dynamical system whose fixed points, either stable or unstable, represent the laminar state and any statistically steady turbulent states. We find that the behaviour of the system depends on the Rayleigh discriminant (defined by equation (3.6)) of the rotating shear flow. The model predicts that Rayleigh-unstable flows become turbulent at sufficiently large Reynolds number through a linear instability associated with a supercritical (or, rarely, subcritical) bifurcation. Flows that are Rayleigh-stable by a sufficiently large margin are predicted not to support sustained turbulence however large the Reynolds number. This behaviour is naturally consistent with Rayleigh's stability criterion.

https://doi.org/10.1017/S002211200500368X Published online by Cambridge University Press

Non-rotating (Rayleigh-neutral) shear flows and those that are Rayleigh-stable by a sufficiently small margin can become turbulent through a nonlinear instability associated with a subcritical bifurcation from infinite Reynolds number. In the non-rotating case the laminar state admits algebraically growing infinitesimal disturbances that are damped only on the viscous time scale Re/S. The nonlinear terms of the model allow perturbations of finite amplitude to be sustained and the system evolves to a non-trivial state of statistically steady turbulence. This behaviour of the model strongly resembles the theory of subcritical transition to turbulence, developed by Trefethen *et al.* (1993) and others, involving the transient amplification of disturbances by a non-normal operator and a cooperative nonlinear feedback. The closure model that we work with has the advantage of being able to represent the final turbulent outcome of the transition process.

The analysis of Reynolds-stress models in homogeneous shear flow in terms of a nonlinear dynamical system is not unique to our work (see e.g. Speziale, Gatski & Mac Giolla Mhuiris 1990). However, the simplicity of our model permits an exhaustive study of its dynamical properties and, by including the effects of a finite Reynolds number, we are able to make a connection with the theory of subcritical transition to turbulence in which the laminar state has a basin of attraction that diminishes as the Reynolds number is increased. Similar techniques of analysis could of course be applied to more sophisticated closure models and we believe that our findings are to some extent generic.

The turbulent solutions are anisotropic as a result of shear and rotation, and in the limit of large Reynolds number the shear stress behaves as in Prandtl's mixing-length theory, but with a prefactor that depends on the Rayleigh discriminant (see equation (3.15)). As such, our model naturally captures the reduction, and eventually suppression, of the turbulent energy dissipation for rapidly rotating flows (Speziale *et al.* 1998).

When applied to wall-bounded turbulent shear flows (§ 3.2), the model predicts the occurrence of a universal velocity profile close to a wall at large Reynolds number. Outside the viscous sublayer, this profile has the logarithmic form predicted by Prandtl's mixing-length theory, and we derive two accurate constraints on the three parameters from matching the most recent experimental data (Zagarola & Smits 1998).

We have also investigated in some detail the predictions of the model for the occurrence and the characteristics of turbulent states in Couette–Taylor flow without end effects (§ 4). Here, depending on the ratios of the radii and angular velocities of the two cylinders, the distribution of the Rayleigh discriminant of the laminar solution may be such that a local analysis would predict either linear instability or nonlinear instability or complete stability in different regions of the flow. Furthermore, once turbulence sets in, the angular velocity distribution and the corresponding Rayleigh discriminant are significantly modified from those of the laminar solution. Therefore a wide variety of behaviour is possible, including the existence of mixed states, in which the turbulence is localized. It is worth noting that although we have restricted the present analysis to solutions of maximal symmetry in the Couette–Taylor system, our model may admit classes of more general solutions. For instance, relaxing the assumption of azimuthal and axial translational symmetry could in principle help explain observed phenomena such as spiral turbulence (Coles 1965; Hegseth *et al.* 1989) in which regions of laminar and turbulent flows coexist separated by a helical interface.

By fitting the remaining parameter of our model, we are able to account quite well for the qualitative behaviour and quantitative torque measurements in

https://doi.org/10.1017/S002211200500368X Published online by Cambridge University Press

historical experiments on Couette–Taylor flow by Wendt (1933) and Taylor (1936*a*), which have not been superseded. As an unexpected bonus, the model captures reasonably accurately the appearance of Taylor vortices at the onset of linear instability.

It is appropriate to discuss at this point some of the implications of the parameterization used in our model. The ratio C_2/C_1 represents the propensity of the turbulence to return to isotropy. In a local analysis, it is found to determine the critical value of the dimensionless Rayleigh discriminant for which high-Reynolds-number turbulence can be sustained. Why these properties should be related can be explained with reference to the system of equations (3.3). When the Rayleigh discriminant $\Phi = 2\Omega(2\Omega - S)$ is positive, the terms $4\Omega R_{xy}$ and $2(S - 2\Omega)R_{xy}$ in the equations for R_{xx} and R_{yy} have opposite signs. Therefore either R_{xx} or R_{yy} lacks a positive source, and the turbulence must decay, unless the C_2 term comes into play. For a given positive Rayleigh discriminant, the isotropizing tendency must be sufficiently great if the turbulence is to be sustained.

In this work, although we have proposed values of the coefficients C_1, C_2 and C_ν after fitting experimental data, these values are only tentative and approximate and we do not claim that such a simple model can provide great quantitative accuracy in comparison with currently available closure models (cf. Choi & Lumley 2001). In particular, the ratio C_2/C_1 is only weakly constrained through a comparison with Wendt's (1933) data, with a wide plausible range of roughly 0.4 to 1.

We draw attention again to the important problem of the hydrodynamic stability of circular Keplerian motion in astrophysical accretion disks, in which the angular velocity profile $\Omega \propto r^{-3/2}$ is enforced by gravitational dynamics, not through the boundaries. While Richard & Zahn (1999) sought to apply the findings of Couette–Taylor experiments to accretion disks, our investigation of turbulent Couette–Taylor flows suggests that caution is required in making such associations. According to our model (taking $C_2/C_1 < 8/3$), Keplerian rotation is likely not to support statistically steady turbulence in a local analysis, and may be nonlinearly stable no matter how large the Reynolds number. We also find that this does not contradict the experimental finding that Couette–Taylor flow with a stationary inner cylinder becomes turbulent at large Reynolds number, and is even consistent with the possibility that a wide-gap Couette–Taylor flow with the cylinders in a Keplerian ratio may be turbulent. In addition, Couette–Taylor experiments are always contaminated to some degree by end effects. We suggest that Couette–Taylor experiments may be of limited applicability to the study of the nonlinear stability of Keplerian rotation, and that it can be instead most usefully addressed in local numerical models such as that of the shearing box (e.g. Balbus & Hawley 1998), which are free from end effects and also from the type of radial boundary conditions that induce boundary layers. To date, no instability has been found in such models, and it would be valuable to test this finding to very high Reynolds numbers.

Finally, we emphasize that the philosophy behind the construction of simple turbulence models such as the one adopted here is applicable to a range of more complex problems such as magnetohydrodynamic turbulence (Ogilvie 2003), convection, or mixing in stratified shear flows. Such extension is the subject of current investigations.

P. G. acknowledges the support of New Hall and PPARC. G. I. O. acknowledges the support of the Royal Society through a University Research Fellowship.

https://doi.org/10.1017/S002211200500368X Published online by Cambridge University Press

Appendix A. Model equations in a general orthogonal curvilinear coordinate system

Using Batchelor's (1967) notation, the equivalent of equation (2.8) for the evolution of the Reynolds stress tensor in general orthogonal curvilinear coordinates is

$$\begin{aligned}\frac{\partial R_{ij}}{\partial t} + \sum_k \Bigg[& \frac{\bar{u}_k}{h_k}\frac{\partial R_{ij}}{\partial x_k} + \frac{R_{kj}}{h_k}\frac{\partial \bar{u}_i}{\partial x_k} + \frac{R_{ik}}{h_k}\frac{\partial \bar{u}_j}{\partial x_k} + \frac{\bar{u}_i R_{kj}}{h_i h_k}\frac{\partial h_i}{\partial x_k} + \frac{\bar{u}_k R_{ij}}{h_i h_k}\frac{\partial h_i}{\partial x_k} \\ & + \frac{\bar{u}_j R_{ik}}{h_j h_k}\frac{\partial h_j}{\partial x_k} + \frac{\bar{u}_k R_{ij}}{h_j h_k}\frac{\partial h_j}{\partial x_k} - 2\frac{\bar{u}_k R_{kj}}{h_i h_k}\frac{\partial h_k}{\partial x_i} - 2\frac{\bar{u}_k R_{ki}}{h_j h_k}\frac{\partial h_k}{\partial x_j}\Bigg] \\ & = -C_1 L^{-1} R^{1/2} R_{ij} - C_2 L^{-1} R^{1/2}\left(R_{ij} - \tfrac{1}{3} R \delta_{ij}\right),\end{aligned} \tag{A 1}$$

where (h_1, h_2, h_3) is $(1, 1, 1)$ for Cartesian coordinates (x, y, z), or $(1, r, 1)$ for cylindrical coordinates (r, ϕ, z).

In the Cartesian case, the viscous correction terms follow from the decomposition

$$\nu(u'_{i,kk}u'_j + u'_{j,kk}u'_i) = \nu((u'_i u'_j)_{,kk} - 2u'_{i,k}u'_{j,k}), \tag{A 2}$$

where the first term on the right-hand side describes a viscous diffusion of the stresses and the second term describes a direct decay of the stresses, which we then model as $-C_\nu \nu R_{ij}/L^2$.

In order to obtain the form for the viscous corrections in general curvilinear coordinates, we follow the same method used in the Cartesian case: we isolate from the original terms $\nu(\nabla^2 u')_i u'_j + \nu(\nabla^2 u')_j u'_i$ the tensor decay term $-2\nu(\nabla \boldsymbol{u}' \nabla^T \boldsymbol{u}')_{ij}$ (which is the covariant equivalent of $-2\nu u'_{i,k}u'_{j,k}$), where $\nabla \boldsymbol{u}'$ is the matrix defined by its columns

$$(\nabla \boldsymbol{u}') = \left(\frac{1}{h_1}\frac{\partial \boldsymbol{u}'}{\partial x_1}, \frac{1}{h_2}\frac{\partial \boldsymbol{u}'}{\partial x_2}, \frac{1}{h_3}\frac{\partial \boldsymbol{u}'}{\partial x_3}\right). \tag{A 3}$$

In this expression, $\boldsymbol{u}' = u'_1\boldsymbol{e}_1 + u'_2\boldsymbol{e}_2 + u'_3\boldsymbol{e}_3$ and the derivatives of the unit vectors $(\boldsymbol{e}_1, \boldsymbol{e}_2, \boldsymbol{e}_3)$ are given by Batchelor (1967, p. 598). We model the decay terms as $-C_\nu \nu R_{ij}/L^2$, and keep the remaining diffusion terms unchanged thereby defining the Laplacian of the second-rank tensor $(\nabla^2 R)_{ij}$. Hence with this method the viscous terms in equation (2.9) are then simply

$$-\frac{C_\nu \nu}{L^2} R_{ij} + \nu(\nabla^2 R)_{ij}, \tag{A 4}$$

with

$$\left.\begin{aligned}(\nabla^2 R)_{rr} &= \nabla^2 R_{rr} - \frac{4}{r^2}\frac{\partial R_{r\phi}}{\partial \phi} + \frac{2}{r^2}(R_{\phi\phi} - R_{rr}), \\ (\nabla^2 R)_{\phi\phi} &= \nabla^2 R_{\phi\phi} + \frac{4}{r^2}\frac{\partial R_{r\phi}}{\partial \phi} + \frac{2}{r^2}(R_{rr} - R_{\phi\phi}), \\ (\nabla^2 R)_{zz} &= \nabla^2 R_{zz}, \\ (\nabla^2 R)_{r\phi} &= \nabla^2 R_{r\phi} + \frac{2}{r^2}\frac{\partial}{\partial \phi}(R_{rr} - R_{\phi\phi}) - \frac{4}{r^2}R_{r\phi}, \\ (\nabla^2 R)_{rz} &= \nabla^2 R_{rz} - \frac{2}{r^2}\frac{\partial R_{\phi z}}{\partial \phi} - \frac{R_{rz}}{r^2}, \\ (\nabla^2 R)_{\phi z} &= \nabla^2 R_{\phi z} + \frac{2}{r^2}\frac{\partial R_{rz}}{\partial \phi} - \frac{R_{\phi z}}{r^2},\end{aligned}\right\} \tag{A 5}$$

in cylindrical coordinates for instance.

https://doi.org/10.1017/S0022112005003680X Published online by Cambridge University Press

For an axisymmetric flow with translational symmetry in z and $\bar{\boldsymbol{u}} = r\Omega(r)\,\boldsymbol{e}_\phi$ in a cylindrical geometry the evolution equations for the Reynolds stress tensor are

$$\left.\begin{aligned}
&\frac{\partial R_{rr}}{\partial t} - 4\Omega R_{r\phi} = -\frac{C_1+C_2}{L}R^{1/2}R_{rr} + \frac{C_2}{3L}R^{3/2} - \frac{\nu C_\nu}{L}R_{rr} + \nu(\nabla^2 R)_{rr},\\
&\frac{\partial R_{\phi\phi}}{\partial t} + 2(2\Omega - S)R_{r\phi} = -\frac{C_1+C_2}{L}R^{1/2}R_{\phi\phi} + \frac{C_2}{3L}R^{3/2} - \frac{\nu C_\nu}{L}R_{\phi\phi} + \nu(\nabla^2 R)_{\phi\phi},\\
&\frac{\partial R_{zz}}{\partial t} = -\frac{C_1+C_2}{L}R^{1/2}R_{zz} + \frac{C_2}{3L}R^{3/2} - \frac{\nu C_\nu}{L}R_{zz} + \nu(\nabla^2 R)_{zz},\\
&\frac{\partial R_{r\phi}}{\partial t} + (2\Omega - S)R_{rr} - 2\Omega R_{\phi\phi} = -\frac{C_1+C_2}{L}R^{1/2}R_{r\phi} - \frac{\nu C_\nu}{L}R_{r\phi} + \nu(\nabla^2 R)_{r\phi},\\
&\frac{\partial R_{rz}}{\partial t} - 2\Omega R_{\phi z} = -\frac{C_1+C_2}{L}R^{1/2}R_{rz} - \frac{\nu C_\nu}{L}R_{rz} + \nu(\nabla^2 R)_{rz},\\
&\frac{\partial R_{\phi z}}{\partial t} + (2\Omega - S)R_{rz} = -\frac{C_1+C_2}{L}R^{1/2}R_{\phi z} - \frac{\nu C_\nu}{L}R_{\phi z} + \nu(\nabla^2 R)_{\phi z},
\end{aligned}\right\} \tag{A 6}$$

where

$$S = -r\frac{\mathrm{d}\Omega}{\mathrm{d}r}. \tag{A 7}$$

Appendix B. Asymptotic solution of the turbulent Couette–Taylor flow for large Reynolds number and large Rossby number

In the limits of large Rossby number (as expected for a small gap) and large Reynolds number, the angular momentum equation (4.2) can be approximated (to first order in Ro^{-1}) by

$$r^2\kappa^2L^2S|S| + 2r^2\kappa^2L^2\Omega|S|\frac{9C_1}{C_2} = \frac{T}{2\pi h\rho}, \tag{B 1}$$

where κ is the von Kármán constant defined in equation (3.28). This provides a quadratic equation for S which can be inverted, and yields (in the same limit)

$$S = -r\frac{\mathrm{d}\Omega}{\mathrm{d}r} = -\frac{9C_1}{C_2}\Omega + \mathrm{sign}(S)\frac{1}{rL(r)\kappa}\sqrt{\frac{|T|}{2\pi h\rho}}. \tag{B 2}$$

This equation must be integrated separately in each interval $(r_i, r_m]$ and $[r_m, r_o)$: in $(r_i, r_m]$,

$$\Omega(r_m)r_m^{-9C_1/C_2} - \Omega(r)r^{-9C_1/C_2} = -\frac{\mathrm{sign}(S)}{\kappa}\sqrt{\frac{|T|}{2\pi h\rho}}\int_r^{r_m}\frac{r'^{-2-9C_1/C_2}}{r'-r_i}\,\mathrm{d}r', \tag{B 3}$$

and in $[r_m, r_o)$,

$$\Omega(r)r^{-9C_1/C_2} - \Omega(r_m)r_m^{-9C_1/C_2} = -\frac{\mathrm{sign}(S)}{\kappa}\sqrt{\frac{|T|}{2\pi h\rho}}\int_{r_m}^{r}\frac{r'^{-2-9C_1/C_2}}{r_o-r'}\,\mathrm{d}r'. \tag{B 4}$$

Let $\alpha = 9C_1/C_2 + 2$. The integrals in equations (B 3) and (B 4) have a logarithmic

https://doi.org/10.1017/S002211200500368X Published online by Cambridge University Press

singularity as $r \to r_i$ and $r \to r_o$, which can be isolated as

$$\int_r^{r_m} \frac{r'^{-\alpha}}{r'-r_i}\,\mathrm{d}r' = f(r;r_m,r_i,\alpha) - r_i^{-\alpha}\ln\left(\frac{r-r_i}{r_m-r_i}\right). \tag{B 5}$$

This defines the function f uniquely. The logarithmic singularity naturally matches onto the boundary layer solutions near the walls.

We use the results of § 3.2 to write the boundary layer solution explicitly. Near $r = r_i$, but outside the viscous sublayer,

$$\Omega(r) = \Omega_i - \frac{\mathrm{sign}(S)}{r_i^2}\sqrt{\frac{|T|}{2\pi h\rho}}\left[v_0(C_1,C_2,C_v) + \frac{1}{\kappa}\ln\left(\frac{r-r_i}{r_i\nu}\sqrt{\frac{|T|}{2\pi h\rho}}\right)\right], \tag{B 6}$$

whereas near $r = r_o$,

$$\Omega(r) = \Omega_o + \frac{\mathrm{sign}(S)}{r_o^2}\sqrt{\frac{|T|}{2\pi h\rho}}\left[v_0(C_1,C_2,C_v) + \frac{1}{\kappa}\ln\left(\frac{r_o-r}{r_o\nu}\sqrt{\frac{|T|}{2\pi h\rho}}\right)\right]. \tag{B 7}$$

Matching the inner (B 6), (B 7) and outer (B 3), (B 4) solutions near the walls, and continuity across the mid-point r_m provides an equation for the torque, which extends the Prandtl–von Kármán skin-friction law for Couette–Taylor flows:

$$\frac{1}{\sqrt{C_f}} = N\log_{10}(Re\sqrt{C_f}) + M, \tag{B 8}$$

where we have defined† $Re = |\Omega_i - \Omega_o|(r_o^2 - r_i^2)/(2\nu)$, $C_f = T/Re^2\rho h\nu^2$ and the friction law coefficients M and N as

$$\left.\begin{aligned} N &= \frac{\mathrm{sign}(S)}{2\kappa\sqrt{2\pi}}\frac{|\Omega_i-\Omega_o|(r_o^2-r_i^2)}{\Omega_i r_i^{2-\alpha} - \Omega_o r_o^{2-\alpha}}\left(r_i^{-\alpha}+r_o^{-\alpha}\right)\ln 10,\\ M &= \frac{\mathrm{sign}(S)}{2\kappa\sqrt{2\pi}}\frac{|\Omega_i-\Omega_o|(r_o^2-r_i^2)}{\Omega_i r_i^{2-\alpha} - \Omega_o r_o^{2-\alpha}}\left[\left(r_i^{-\alpha}+r_o^{-\alpha}\right)\left(\ln\frac{r_o-r_i}{\sqrt{8\pi}} + \kappa v_0(C_1,C_2,C_v)\right)\right.\\ &\quad \left. + \left(f(r_i;r_m,r_i,\alpha) + f(r_o;r_m,r_o,\alpha)\right) - \left(\frac{\ln r_i}{r_i^\alpha} + \frac{\ln r_o}{r_o^\alpha}\right)\right]. \end{aligned}\right\} \tag{B 9}$$

Note that in the limit where the contribution from rotation on the Reynolds stresses is neglected ($Ro^{-1} = 0$), the solution in the bulk of the fluid can be written out as equations (B 3) and (B 4) with $\alpha = 2$ and

$$f(r;r_m,r_i,2) = \frac{1}{r_i^2}\left(\frac{1}{r_m} - \frac{1}{r} + \ln r - \ln r_m\right). \tag{B 10}$$

In figure 15 we compare the velocity profiles obtained by numerical integration to those derived from asymptotic analysis, for three different gap widths. We find that the asymptotics only provide accurate results for $d/r_o \leqslant 0.02$. This somewhat disappointing range of applicability of the $Ro \gg 1$ asymptotic analysis is due to the great efficiency with which turbulence redistributes the shear, which reduces the Rossby number in the interior of the flow compared to that of the laminar solution.

† Other authors who use a different definition of the Reynolds number Re^* obtain skin-friction law coefficients M^* and N^* which are related to ours through the expression $M^* = (Re^*/Re)M$ and $N^* = (Re^*/Re)N$.

https://doi.org/10.1017/S0022112005003680X Published online by Cambridge University Press

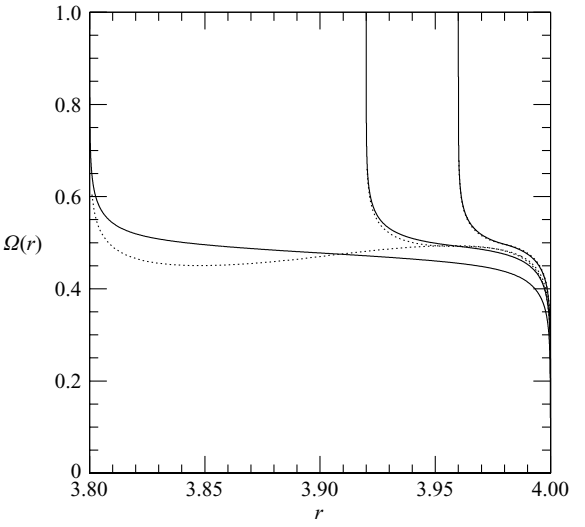


FIGURE 15. Comparison between complete numerical solution (solid line) and asymptotic analytical solution (dotted line) for three gap widths $d/r_o = 0.05$, 0.02 and 0.01 respectively, for a Reynolds number of the flow $Re = 10^6$.

REFERENCES

ANDERECK, C. D., LIU, S. S. & SWINNEY, H. L. 1986 Flow regimes in a circular Couette system with independently rotating cylinders. *J. Fluid Mech.* **164**, 155–183.

BAGGETT, J. S. & TREFETHEN, L. N. 1997 Low-dimensional models of subcritical transition to turbulence. *Phys. Fluids* **9**, 1043–1053.

BALBUS, S. A. & HAWLEY, J. F. 1998 Instability, turbulence, and enhanced transport in accretion disks. *Rev. Mod. Phys.* **70**, 1–53.

BATCHELOR, G. K. 1967 *An Introduction to Fluid Dynamics.* Cambridge University Press.

BOUSSINESQ, J. 1877 Essai sur la théorie des eaux courantes. *Mém. Acad. Sci. Paris* **23**, 1–660.

BUTLER, K. M. & FARRELL, B. F. 1992 Three-dimensional optimal perturbations in viscous shear flow. *Phys. Fluids* A **4**, 1637–1650.

CHOI, K. S. & LUMLEY, J. L. 2001 The return to isotropy of homogeneous turbulence. *J. Fluid Mech.* **436**, 59–84.

COLES, D. 1965 Transition in circular Couette flow. *J. Fluid Mech.* **21**, 385–425.

DAUCHOT, O. & DAVIAUD, F. 1995 Finite amplitude perturbation and spot growth mechanism in plane Couette flow. *Phys. Fluids* **7**, 335–343.

DRAZIN, P. G. & REID, W. H. 1981 *Hydrodynamic Stability.* Cambridge University Press.

FRANK, J., KING, A. & RAINE, D. 2002 *Accretion Power in Astrophysics,* 3rd edn. Cambridge University Press.

GROSSMANN, S. 2000 The onset of shear flow turbulence. *Rev. Mod. Phys.* **72**, 603–618.

HEGSETH, J. J., ANDERECK, C. D., HAYOT, F. & POMEAU, Y. 1989 Spiral turbulence and phase dynamics. *Phys. Rev.* E **62**, 257–260.

LATHROP, D. P., FINEBERG, J. & SWINNEY, H. L. 1992 Transition to shear-driven turbulence in Couette–Taylor flow. *Phys. Rev.* A **46**, 6390–6405.

LAUNDER, B. E., REECE, G. J. & RODI, W. 1975 Progress in the development of a Reynolds stress turbulence closure. *J. Fluid Mech.* **68**, 537–566.

LEWIS, G. S. & SWINNEY, H. L. 1999 Velocity structure functions, scalings, and transition in high-Reynolds-number Couette–Taylor flow. *Phys. Rev.* E **59**, 5457–5467.

MCKEON, B. J., JIANG, W., MORRISON, J. F. & SMITS, A. J. 2003 Pitot probe corrections in fully developed turbulent pipe flow. *Meas. Sci. Technol.* **14**, 1449–1458.

NAGATA, M. 1990 Three-dimensional finite-amplitude solutions in plane Couette flow: bifurcation from infinity. *J. Fluid Mech.* **217**, 519–527.

https://doi.org/10.1017/S002211200500368X Published online by Cambridge University Press

Ogilvie, G. I. 2003 On the dynamics of magnetorotational turbulent stresses. *Mon. Not. R. Astron. Soc.* **340**, 969–982.

Prandtl, L. 1925 Bericht über Untersuchungen zur ausgebildeten Turbulenz. *Z. Angew. Math. Mech.* **5**, 136–139.

Pringle, J. E. 1981 Accretion discs in astrophysics. *Annu. Rev. Astron. Astrophys.* **19**, 137–162.

Pumir, A. 1996 Turbulence in homogeneous shear flows. *Phys. Fluids* **8**, 3112–3127.

Rayleigh, Lord 1917 On the dynamics of revolving fluids. *Proc. R. Soc. Lond.* A **93**, 148–154.

Reichardt, H. 1940 Die Wärmeübertragung in turbulenten Reibungsschichten. *Z. Angew. Math. Mech.* **20**, 297–328.

Reynolds, O. 1895 On the dynamical theory of incompressible viscous fluids and the determination of the criterion. *Phil. Trans. R. Soc. Lond.* A **186**, 123–164.

Richard, D. 2001 Instabilités hydrodynamiques dans les écoulements en rotation différentielle. PhD dissertation, Université Paris 7 Denis Diderot.

Richard, D., Dauchot, O., Daviaud, F. & Zahn, J.-P. 2001 Subcritical instabilities of astrophysical interest in Couette–Taylor systems. In *Proc. 12th Couette–Taylor Workshop, Evanston, USA.*

Richard, D. & Zahn, J.-P. 1999 Turbulence in differentially rotating flows: what can be learned from the Couette–Taylor experiment. *Astron. Astrophys.* **347**, 734–738.

Rogallo, R. S. 1981 Numerical experiments in homogeneous turbulence. *NASA Tech. Mem.* TM-81315.

Rotta, J. C. 1951 Statistische Theorie nichthomogener Turbulenz. *Z. Phys.* **129**, 547–572.

Schlichting, H. 1979 *Boundary-layer Theory*, 7th ed. McGraw-Hill.

Schultz-Grunow, F. 1959 Zur Stabilität der Couette-Strömung. *Z. Angew. Math. Mech.* **39**, 101–110.

Sjögren, T. & Johansson, A. V. 2000 Development and calibration of algebraic nonlinear models for terms in the Reynolds stress transport equations. *Phys. Fluids* **12**, 1554–1572.

Speziale, C. G. 1991 Analytical methods for the development of Reynolds-stress closures in turbulence. *Annu. Rev. Fluid Mech.* **23**, 107–157.

Speziale, C. G., Gatski, T. B. & Mac Giolla Mhuiris, N. 1990 A critical comparison of turbulence models for homogeneous shear flows in a rotating frame. *Phys. Fluids* A **2**, 1678–1684.

Speziale, C. G., Younis, B. A., Rubinstein, R. & Zhou, Y. 1998 On consistency conditions for rotating turbulent flows. *Phys. Fluids* **10**, 2108–2110.

Tassoul, J.-L. 1978 *Theory of Rotating Stars.* Princeton University Press.

Taylor, G. I. 1923 Stability of a viscous liquid contained between two rotating cylinders. *Phil. Trans. R. Soc. Lond.* A **223**, 289–343.

Taylor, G. I. 1936*a* Fluid friction between rotating cylinders. I. Torque measurements. *Proc. R. Soc. Lond.* A **157**, 546–564.

Taylor, G. I. 1936*b* Fluid friction between rotating cylinders. II. Distribution of velocity between concentric cylinders when outer one is rotating and inner one is at rest. *Proc. R. Soc. Lond.* A **157**, 565–578.

Thomson, W. (Lord Kelvin) 1887 Stability of fluid motion — rectilineal motion of viscous fluid between two parallel planes. *Phil. Mag.* **24** (5), 188–196.

Trefethen, L. N., Trefethen, A. E., Reddy, S. C. & Driscoll, T. A. 1993 Hydrodynamic stability without eigenvalues. *Science* **261**, 578–584.

Waleffe, F. 1997 On a self-sustaining process in shear flows. *Phys. Fluids* **9**, 883–900.

Wendt, F. 1933 Turbulente Strömungen zwischen zwei rotierenden konaxialen Zylindern. *Ing. Archiv* **4**, 577–595.

Zagarola, M. V. & Smits, A. J. 1998 Mean-flow scaling of turbulent pipe flow. *J. Fluid Mech.* **373**, 33–79.

https://doi.org/10.1017/S002211200500368X Published online by Cambridge University Press